Technical University of Denmark

DTU

Fibers for 160 Gbit/s Transmission and above

Le, Nghi Trong Quang; Jeppesen, Palle

Publication date:
2003

Document Version
Publisher's PDF, also known as Version of record

Link back to DTU Orbit

DTU Library
Technical Information Center of Denmark

Fibres For 160Gbit/s Transmission And Above

Thesis for industrial Ph.D.

Le Nghi Trong <u>Quang</u>

EF869/938441 (PHD)

June 17, 2003
Revised October 31, 2003

Parties supporting this work

PREFACE

This thesis is submitted to the Technical University (DTU) of Denmark and the Danish Academy of Technical Sciences (ATV) for partial fulfillment of the requirements to the industrial Ph.D. education. The work was done in the period June 2000 to May 2003. A four month stay at the Heinrich Hertz Institute in Berlin from October 2002 to January 2003 was carried out successfully.

The work was done at specialty fiber devices at Lucent Technologies Denmark I/S now OFS Fitel Denmark I/S (Since November 2001), and COM Centre at the Technical University of Denmark. The supervisor were Prof. Dr. Tech. Palle Jeppesen from COM Centre, Dr. Lars Grüner-Nielsen, and VP. Dr. C. Christian Larsen both the latter are from OFS Fitel Demark I/S.

The work has resulted in 9 refereed papers. A list of papers is given on page xi.

Le Nghi Trong Quang

—It is not embarrassing to fail.
Failing to learn from ones failures is embarrassing
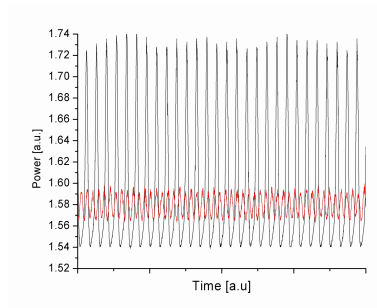
160Gbit/s (black) and 320Gbit/s (red) pulse trains.
COM, February 2003

ABSTRACT

The topic of the work presented in this thesis is fibres for 160Gbit/s transmission and above. This thesis entails three parts. First the dispersion compensation requirements and related topics are investigated. Secondly fibre non-linearity is considered with an emphasis on Raman amplification. And last system experiments have been performed.

The effect of chromatic dispersion is briefly described and higher order chromatic dispersion is examined in order to establish their relative influence on transmission quality. The pulse distortions of the higher order dispersion can be understood from very simple physical considerations. Dispersion compensation is investigated in order to determine the requirements for dispersion and slope compensation. Tolerance to dispersion and slope of a system is established from basic principles deduced from the non-linear Schrödinger equation. Design targets for the dispersion compensating fibres in terms of slope compensation is explored. Finally the issue of determining the dispersion slope and possible curvature of the dispersion compensating fibre has been investigated.

Fibre non-linearity pose a threat to system performance and is investigated. In particular Raman enhanced non-linearity is considered since distributed Raman amplification is being widely deployed in laboratories and in the field. However Raman pumping of the dispersion compensating module, i.e discrete Raman amplification, is also emerging, thus making it important to understand the effects of Raman amplification on the non-linearity.

System experiments has been performed at both 40Gbit/s and 160Gbit/s using the return to zero, RZ, format. Only single channel experiments are considered in this thesis. The experiments at 160Gbit/s were done on four different types of fibres to compare the performance of the fibres. Raman amplification was tested in the 40Gbit/s experiments and 1280km of transmission was obtained with Raman.

RESUMÉ

Emnet for det i denne afhandling præsenterede arbejde er optiske fibre til brug ved transmissionshastigheder på 160Gbit/s eller derover. Afhandlingen udgøres af tre hovedemner. Først bliver forudsætningerne for dispersion kompensering samt relaterede spørgsmål undersøgt. Dernæst ses der på fiber ikke-lineariteterne, med vægt på forstærkning via Raman effekten. Afslutningsvis bliver de udførte systemforsøg beskrevet.

Effekten af kromatisk dispersion bliver beskrevet kort. Højere ordens dispersion bliver undersøgt med det mål at bestemme deres indflydelse på transmissionskvaliteten af systemerne. Forvrængningerne fra højere ordens dispersionen kan forstås ud fra ganske simple fysiske principper. Dispersionskompensering bliver undersøgt, for at kunne bestemme kravene til dispersionskompensering samt kompensering for dennes gradient. Dispersions og gradienttolerancen af systemerne bliver estimeret fra basale principper udledt af den ikke-lineære Schrødinger ligning. Designmål for dispersionskompenserende fibre med henblik på gradient kompensering bliver undersøgt. Sidst bliver der set på bestemmelsen af dispersion samt gradienten og muligvis krumningen vha. eksperimentelle målinger.

Fiber ikke-lineariteter kan forringe systemernes ydeevne og bliver derfor undersøgt. Især vil Raman effektens indflydelse på ikke-lineariteterne være interessant, idet "fordelt" forstærkning via Raman effekten er vidt udbredt. Brugen af Raman effekten til forstærkning bliver i stigende grad også udbredt til at foregå i den dispersionskompenserende fiber, hvilket forstærker behovet for at forstå Raman effektens indflydelse på ikke-lineariteterne.

Systemeksperimenter har været foretaget ved både 40Gbit/s og 160Gbit/s i "return to zero" RZ formatet. Kunenkelt kanals OTDM forsøg bliver beskrevet. For at sammenligne ydelsen af forskellige fibre blev 160Gbit/s forsøgene udført med fire forskellige sæt af fibre. Forstærkning via Raman effekten blev undersøgt ve 40Gbit/s forsøgene.

ACKNOWLEDGEMENTS

I am very grateful to a number of people without whom some of the work presented in this thesis would not have been possible. At OFS Fitel Denmark where most of the time was spend I cherished the interaction with the colleagues. I worked closely with a number colleagues and would like to thank Carsten G. Jørgensen, Yujun Qian, Stig Nissen Knudsen, Morten Ø. Pedersen, Poul Kristensen, Tommy Geissler, Jacob Rathje, Marie Wandel, and Peter Gaarde just to mention a few.

A special thanks to Professor H.G. Weber at HHI, Berlin, and his group, with whom I visited for four very fruitful months. Your guidance and supervision during my stay was greatly respected and appreciated. To the colleagues at HHI I would like to thank you all for making the stay pleasant, also outside working hours. I worked closely and learned a lot from Jörn Berger, Sebastian Ferber, and Vincent Marembert. Furthermore Enno Hilliger and Marcel Kroh are appreciated for their help around the office.

I have been very fond of the atmosphere among the colleagues at COM and benefited greatly from the stimulating intellectual environment at COM. In particular I would like to thank all the colleagues at the Systems Group at COM for there readiness to help when help was needed. In particular I would like to express my gratitude to Christophe Peucheret, Torge Tokle, Jorge Seoane, and Kim Skaalum Berg for a fruitful cooperation and for your friendship.

To my supervisors I would like to express a great thanks for their kind supervision and great patience. To Palle Jeppesen my supervisor at COM your subtle and insightful guidance has been a great help at all times. To Christian Larsen your support and interest in my work has been very rewarding. And Lars Grüner-Nielsen your keen supervision, hints and interest was appreciated with utmost respect.

I would also like to express my thanks to my brother Thanh, sisters Phuc Duyen, Tu Duyen, An, and finally friend and brother in law Henrik for your support and help during the course of the work; I owe you two. A thanks to Helene for supporting me and offering to do my laundry. Finally my parents

must be thanked for giving me this opportunity and the drive to continue—Your sacrifice made it possible.

LIST OF PUBLICATIONS

A J. Berger, **Q. Le**, A. Wietfeld, S. Ferber, L. Grüner-Nielsen, B. Schmauss, H.G. Weber. *160 Gbit/s Transmission over Dispersion Managed Fibre Set.* Accepted for oral presentation at European Conference on Optical Communication, ECOC 2003, Rimini, Italy.

B Yujun Qian, **Quang Le**, Wenfeng Wang, Bera Pálsdóttir, Carsten G. Jørgensen. *Optimized dispersion compensating Raman amplifier with respect to linear and nonlinear impairments*, Technical Digest of conference on Optical Fibre Communication, OFC 2003

C **Quang Le N.T.** , Carsten Gudmann Jørgensen , Lars Grüner-Nielsen, Bera Pálsdóttir. *Enhancement of Non-Linear Response of a Highly Non-Linear Fibre Due to Raman Amplification.* Proceedings of European Conference on Optical Communication, ECOC 2002; paper 3.2.5.

D Marie Wandel, Poul Kristensen, Torben Veng, Yujun Qian, **Quang Le** , Lars Grüner-Nielsen. *Dispersion Compensating Fibers for Non-Zero Dispersion Fibers.* Technical Digest of conference on Optical Fibre Communication, OFC 2002 Paper WU1. pp.327-329.

E L. Leng, **Quang Le N.T.** , Lars Grüner-Nielsen, B. Zhu, S. Stulz, and L. E. Nelson. *1.6 Tb/s (40 x 40 Gb/s) Transmission over 500 km of Non-Zero Dispersion Fiber with 100-km Amplified Spans Compensated by Extra-High-Slope Dispersion-Compensating Fiber.* Technical Digest of conference on Optical Fibre Communication, OFC 2002 Paper ThX2.

F Zhenbo Xu, Christophe Peucheret, **Quang Le N.T.** , Palle Jeppesen. *Short Period Dispersion Management of 160 Gb/s Single Channel Fiber Systems* . Proceedings of European Conference on Optical Communication, ECOC 2002; paper P3.15.

G Marie Wandel, Torben Veng, **Quang Le N.T.** , Lars Grüner-Nielsen. *Dispersion Compensating Fibre With a High Figure of Merit.* Proceedings of European Conference on Optical Communication, ECOC 2001; paper PD.A.1.4.

H **Quang Le N.T.** , Mads Astrup Hansen. *Measuring Chromatic Dispersion Slope of a Dispersion Compensating Fibre More Accurately using Orthogonal Chebyshev Polynomials.* Optical Fibre Measurement Conference, OFMC 2001, Girton College, Cambridge.

I **Quang Le N.T.** , Torben Veng and Lars Grüner-Nielsen. *New Dispersion Compensating Module for Compensation Of Dispersion and Dispersion Slope of Non-Zero Dispersion Fibres in the C-Band.* Technical Digest of conference on Optical Fibre Communication, OFC 2001 paper TuH5.

CONTENTS

LIST OF FIGURES

LIST OF TABLES

1. INTRODUCTION

In this section a discussion of the scope of the industrial Ph.D. project is given. The project is entitled "Fibres for transmission systems working at 160Gbit/s and above. The project is thus a study of optical fibres in a systems context i.e. to understand the response to the optical field propagating in these fibres. The behaviour is governed by the compositions of the material and the response of the material to an optical field.

Using a phenomenological approach the propagation of an optical pulse in the slowly varying approximation can be described by the non-linear Schrödinger equation. The different terms of this non-linear differential equation represent different physical effects, which are divided into linear effects and non-linear effects. The linear effects are characterized by conservation of energy and momentum, whereas the non-linear effects do not conserve energy. The non-linear effects are proportional to the intensity of the light propagating in the fiber. The non-linear effects of the optical fibres are usually very low compared to the linear, however due to the great distances the effects accumulate and their effects become significant; much in the same sense with the gravitational force, which is the weakest of the four natural forces. The mass of the entire earth exerts a small force on a small paper clip that can be easily exceeded by a magnet with a mass much less than the mass of the earth; yet nobody seems to have floated towards outer space.

Transmission systems are now operating at 10Gbit/s with an expected upgrading to 40Gbit/s in the near future. As the bit rate becomes even faster the tolerance of the systems to the different effects mentioned above becomes smaller and smaller. In other words the significance of the effects becomes larger with the rising of the bit rate. I.e. the higher the bit rate the smaller the time slot of a pulse becomes, however, some minimum power is still needed for detection resulting in a higher non-linearity, due to the increased intensity of the short optical field. At transmission speeds at 160Gbit/s and above these effects can surely not be neglected.

The scope of the project is to obtain knowledge about the requirements for

future high bit rate transmission systems, through simulations of systems and actual systems experiments at very high bit rates.

Reports on high bit rate systems experiments are increasing rapidly in the literature [2, 3]. The focus of these reports has mainly been to show increased capacity of the systems, i.e. [3] reports on a wavelength division multiplexing system working at 160Gbit/s with a high spectral efficiency of $0.53git/(s \cdot Hz)$, where six channels with a 300GHz grid was used. A polarization multiplexing scheme was applied to limit the effects of intra channel cross phase modulation and four wave mixing. A field trial over $116km$ of installed fibre was reported in [2]. [4] reports transmission using an even higher transmission rate of 640Gbit/s over 100km of fibre. A 19 channel experiment with a $160Gbit/s$ line rate was reported in [5] showing an impressive $3Tbit/s$ capacity over $40km$ of fibre.

Due to the limited bandwidth of current high grade electronics ~ 40 GHz all systems operating at higher bit rates than $40Gbit/s$ must use optical time division multiplexing (OTDM) to make the line rate. The work presented in this thesis only focuses on OTDM systems and not wavelength division multiplexing system (WDM) although some were performed. Only pseudo linear transmission will be taken into account.

Dispersion compensation can be realized in a wide variety of methods. In this work the focus has been on single mode dispersion compensating fibres, i.e. fibres with negative dispersion parameters or equivalently fibres with normal dispersion. One of the main advantages of the dispersion compensating fibres is the wide band it can be employed in [1, 6, 7]. In the following a few other methods to compensate for the dispersion in the transmission fibres are mentioned.

Higher order mode dispersion compensating fibres [8, 9, 10]

Phase conjugation [11, 12, 13]

Pre-chirping [14, 15]

Dispersion compensating fibre Bragg gratings [16]

Virtual image phased array devices [17, 18]

Interferometric techniques [19, 20]

The devices given in the list above all show some potential, however so far dispersion compensating fibres have had the lead due to its simplicity and wide broad band compensation. Colleagues at OFS Fitel Denmark have realized

a dispersion compensating module with slope compensation in both C-and L-band. However as the bit rate is increased further the need for single channel and adaptive dispersion compensation will be needed, due to the very tight tolerance of the dispersion of high bit rate systems, opening for a market for some of the devices mentioned above.

Obviously $160Gbit/s$ transmission systems are a prerequisite for the work presented in this thesis, but the question remains: "Do we need systems operating at $160Gbit/s$ or above? The question however is not sought answered in the work. A common argument for working on $160Gbit/s$ technology would be of economical character; it is cheaper than systems based on lower bit rates, due to the smaller amount of channels and thus lower number of expensive components needed by a high bit rate system to encompass same capacity of a low bit rate system. However as this argument was straightforward when systems were upgrading to $10Gbit/s$ and $40Gbit/s$ it is somewhat different in the case of $160Gbit/s$ and above due to the introduction of new component types such as broad band PMD mitigating devices, and adaptive dispersion compensation. There is however a technological argument for working on $160Gbit/s$ transmission systems which at the current time is more applicable than the economical argument. By working on $160Gbit/s$ systems $40Gbit/s$ systems mature faster and become more feasible. This is due to the advance in the 40Gbit/s technology needed in order to realize stable $160Gbit/s$ systems, furthermore much of the technology developed for $160Gbit/s$ systems are applicable also at $40Gbit/s$ increasing the system margin allowing even farther transmission distances. Thus work on $160Gbit/s$ could be a means to reduce the cost of $40Gbit/s$ systems.

1.1 This thesis

In this thesis the requirements for $160Gbit/s$ transmission and above is investigated. Most weight is laid in dispersion compensating fibres and the slope matching requirements. However degrading effects such as polarization mode dispersion will not be discussed in this thesis. This thesis comprises of five chapters. The second chapter discusses chromatic dispersion and related topics. Higher order dispersion is investigated and their influence on transmission system are estimated. The basics of dispersion compensation will be discussed with an emphasis on slope compensation and how a dispersion compensating module should be designed. Measuring the dispersion accurately is also important and will be the topic of the last section in the chapter. The third chapter contains a discussion of Raman enhanced nonlinearity, including an experimental result

on a highly non-linear fibre. Finally systems experiments are presented. In particular a comparison of the performance of different fibre types in a 160Gbit/s transmission experiment is given.

2. DISPERSION COMPENSATION FIBRES

In this chapter the effect of chromatic dispersion and higher order dispersion is investigated. Only the third and fourth order chromatic dispersion is considered. Qualitatively the odd orders of the higher order dispersion have the same effect as the third order dispersion, and likewise for the even orders and the fourth order dispersion [21]. The pulse distortions are explained using basic physical principles. The investigation only considers transform limited pulses, due to the fact that linear chirp is equivalent with second order dispersion; this is shown in appendix B.

The analysis of the chromatic dispersion is done in order to establish a means of deciding the tolerance of a system to second and higher order dispersion. Dispersion compensation using fibres is discussed. The requirements for slope compensation is investigated and the design target for the relative dispersion slope is established. Realized fibres that meet these target are shown. The issue of measuring the dispersion slope is considered at the end of the chapter. Other compensation schemes for higher order dispersion compensation than slope compensation has been reported [22, 23] in literature.

At transmission rates of $160Gbit/s$ the time slot is $6.25ps$. Assuming that the pulse width to time slot ratio—the duty cycle—is in the order of 0.25, the pulse width needed to transmit information at $160Gbit/s$ is $1.56ps$. A further assumption that the pulses are transform limited reveals that the spectral width of the pulses would be $640GHz$ or approximately $5nm$ at $1550nm$. Since $1550nm$ corresponds to $193THz$ it is seen that the bandwidth carrier frequency ratio is $\frac{\Delta\omega}{\omega_0} = 0.3\%$ which validates the slowly varying amplitude approach used to derive the non-linear Schrödinger equation (See appendix A).

The non-linear Schrödinger equation which governs the propagation of pulses with more than $1ps$ duration [24, 25, 26] is given in equation 2.1. For shorter pulses higher order terms of both the linear and non-linear parts may influence the propagation of the pulse and as such should be included in the investigation.

$$(2.1) \quad i\frac{\partial A(z,T)}{\partial z} = -\frac{i}{2}\alpha A(z,T) + \frac{\beta_2}{2}\frac{\partial^2 A(z,T)}{\partial T^2} - \gamma|A(z,T)|^2 A(z,T)$$

where α is the fiber attenuation, and β_2 is the second order chromatic dispersion. The rightmost term in equation 2.1 is a nonlinear term which is originating from the third order susceptibility $\chi^{(3)}$.

$$(2.2) \quad \gamma = 2\frac{\omega_0}{c}\frac{n_2}{A_{eff}}$$

A_{eff} is the effective area. some time called the effective core area in the literature, A_{eff} is however a coupling efficiency parameter, since it is an overlap integral of two mutual interacting fields through the fibre non-linearity [24]. γ is a non-linear coupling coefficient and is responsible for a wide variety of non-linear interactions, such as self phase modulation, SPM, cross phase modulation, XPM, and four wave mixing, FWM. However if $\frac{\gamma P_0 T_0^2}{\beta_2} \ll 1$ the non-linear term can be disregarded since the effect of chromatic dispersion would dominate in equation 2.1. The group velocity dispersion parameter β_2 is defined in equation 2.3 for the case $n = 2$.

$$(2.3) \quad \beta_n = \frac{d^n}{d\omega^n}\beta(\omega)|_{\omega=\omega_0}$$

$\beta(\omega)$ is the effective modal wave number of the fiber. Since the focus of this work has been single mode fibres $\beta(\omega)$ is taken as the wave number of the fundamental mode [27]. β_2 is called the group velocity dispersion parameter due to the fact that $\beta_2 = \frac{d}{d\omega}\frac{1}{v_g}$, with v_g as the group velocity. In the slowly varying envelope approximation, where the optical bandwidth is much smaller than the optical frequency, the propagation constant $\beta(\omega)$ can be approximated by a Taylor expansion around the center frequency, ω_0, as seen in equation 2.4.

$$(2.4) \quad \beta(\omega) = \beta_0 + \beta_1\omega + \frac{1}{2}\beta_2\omega^2 + \frac{1}{6}\beta_3\omega^3 + \frac{1}{24}\beta_4\omega^4 + \dots$$

where β_n is given in equation 2.3. In the slowly varying envelope approximation β_0 is dropped as seen in appendix A. Furthermore the first order term proportional to β_1 in equation 2.4 can be eliminated by using the retarded time, $T = t - \beta_1 z$. In equation 2.4 the angular frequency difference is denoted $\omega = \omega_1 - \omega_0$, where ω_1 is the actual frequency. A traditional Δ denoting differences has been omitted for simplicity of notation.

In the linear case where all fibre non-linearities are neglected the propagation of the optical pulse—or equivalently the slowly varying amplitude of the optical field—through the fibre is governed by equation 2.5.

$$(2.5) \quad i\frac{\partial A(z,T)}{\partial z} = \frac{\beta_2}{2}\frac{\partial^2 A(z,T)}{\partial T^2}$$

which is a special case of the more general non-linear Schrödinger equation 2.1 where the fibre attenuation, α, and non-linearity, γ has been neglected.

2.1   Group velocity dispersion

In this section the effect of group velocity dispersion is surveyed by calculating the propagation of two optical pulses with a Gaussian and a hyperbolic secant, Sech, temporal distribution of the optical power. The calculation is done quite generally by using normalized length and time scales in the linear part of the non-linear Schrödinger equation 2.5 (see appendix A). The physical length is scaled relative to the dispersion length, L_D, of the fibre and the retarded time is measured in units of one initial pulse width, T_0.

(2.6) $L_D = \dfrac{T_0^2}{|\beta_2|}$

L_D is intimately associated with the pulse broadening since for a transform limited pulse $T_0 \Delta \omega_0 = 1$. It can thus be seen that L_D apart from a constant is equivalent to the third term in equation 2.4. So L_D is the length for which the phase of optical field has changed by some amount. Since different frequency components acquire a different phase difference when propagating a certain length due to the second order term in equation 2.4 the pulse is broadened. With the scaled length, $x = \frac{z}{L_D}$, and time, $\tau = \frac{T}{T_0}$, equation 2.7 is rewritten.

(2.7) $i\dfrac{\partial A(x, \tau)}{\partial x} = \dfrac{1}{2}\dfrac{\partial^2 A(x, \tau)}{\partial \tau^2}$

In all the calculations shown in this section a transform limited pulse is used as the initial pulse (see appendix C).

Figure 2.1 shows the effect of the group velocity dispersion. In order to enable a direct comparison between the transmitted pulse and the initial pulse the pulse powers are normalized to the peak power. The transmitted pulse is propagated two dispersion lengths i.e. $x = 2$. It is clear to see that the full width of the pulse at half maximum, FWHM pulse width, has increased for both of the transmitted pulses. For the Gaussian pulse the broadening factor can be expressed analytically. In the simulation the broadening factor was chosen to be $\sqrt{5} \simeq 2.24$. Using a ruler the width of the pulse in figure 2.1(a) is measured to be ~ 2.2 times the initial FWHM pulse width as expected. The pulse broadening of the Sech pulse is measured to be ~ 2.2.

(d) Gauss   (e) Sech
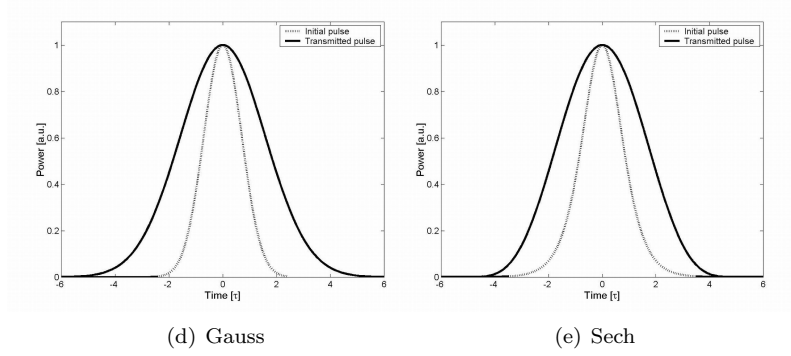
Fig. 2.1: Pulse broadening due to $\beta_2 > 0$ for $x = 2$. The pulses are normalized
to the peak power. The evolution of the Gaussian pulse is shown in
(a) and in (b) the Sech pulse evolution is shown.

(a) Gauss   (b) Sech
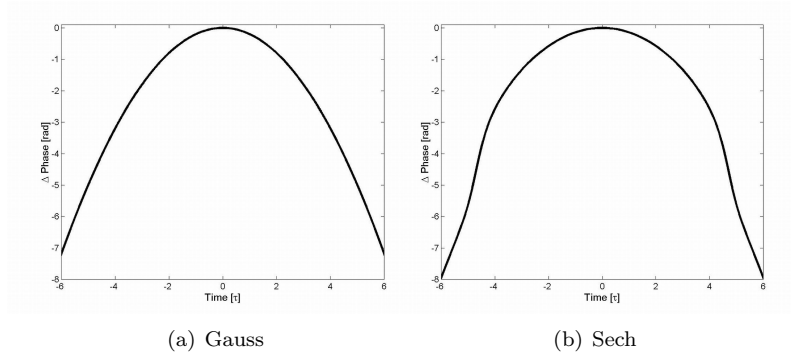
Fig. 2.2: The phase of the Gaussian (a) and Sech (b) pulses shown in figure 2.1
are shown. The phases are given relative to the phase of the peak.

Figure 2.2 shows clearly that the phase measured relatively to the phase at
the peak is changing with the duration of the pulse. For the Gaussian pulse fig-
ure 2.2(a) the phase changes as one would expect from the analytical expression
given in equation 2.8.

$$(2.8) \quad \phi_{\beta_2}(\tau) = -\frac{sign(\beta_2)x\tau^2}{2\sqrt{1+x^2}}$$

where an unimportant constant term has been omitted. The curve of the expression in equation 2.8 is coincident with the curve seen in figure 2.2 and only one curve would show. The chirp is proportional to the temporal changes of the phase i.e. the temporal derivative of the phase. For the Gaussian pulse this chirp is linear. The phase of the Sech pulse is shown in figure 2.2(b). It shows almost same behaviour as the phase of the Gaussian pulse, however there are two steep changes at the sides of the graph causing a non-linear chirp. The phase of the Sech pulse is broader, i.e varying slower, than the phase of the Gaussian pulse in the central part of the pulses. The differences of the phases of the pulses are due to their different spectra. It is thus seen that the phase difference depends strongly on the spectrum of the optical pulse.

2.1.1   Dispersion parameter, D

Instead of the group velocity parameter, β_2 the dispersion parameter, D, is more often used in the optical telecommunication industry. D is the wavelength representation of the group velocity dispersion parameter, i.e the parameter is expressed in the wavelength space instead of the frequency space used so far.

$$(2.9) \quad D = \frac{d}{d\lambda}\frac{1}{v_g} = -\frac{2\pi c}{\lambda^2}\beta_2$$

The dispersion parameter for five different transmission fibre types are given in table 2.1. The different fibre types in table 2.1 are all transmission fibres. The standard single mode, SMF, is the classical unshifted single mode fibre and the super large area, SLA, is the modern version of the SMF where the effective area has been increased to $\sim 110\mu m^2$ compared to $\sim 80\mu m^2$ for the SMF. The latter three fibres are all so-called non-zero dispersion shifted fibres from different manufacturers; The TrueWave-Reduced Slope (TW-RS) is from OFS Fitel, the TeraLight is from Alcatal, and finally the E-LEAF is from Corning. Common for the non-zero disperion fibres is their effective areas are smaller than the effective areas of the non-shifted fibres. The effective areas of the non-zero dispersion shifted fibres are in the range $\sim 50\mu m^2$–$70\mu m^2$ somewhat smaller than the effective area of the SMF. In order to complete table 2.1 the slope if the dispersion parameter, $S = \frac{dD}{d\lambda}$ is given. β_2 is calculated from equation 2.9 using the D parameters from table 2.1.

As seen from table 2.1 the group velocity dispersion parameter of the modern transmission fibre varies in the range $4ps/(nm \cdot km)$–$20ps/(nm \cdot km)$. From the definition of the dispersion length, L_D, it is seen that for a pulse with fixed width of $1.56ps$ the dispersion length of the TW-RS and the LEAF fibres are

	Unit	SLA	SMF	TeraLight	TW-RS	E-LEAF
D	$ps/(nm \cdot km)$	20	17	8	4.5	4.2
S	$ps/(nm^2 \cdot km)$	0.062	0.058	0.058	0.045	0.085
β_2	ps^2/km	−26	−22	−12	−5.8	−5.4

Tab. 2.1: The dispersion parameters at 1550nm for five different transmission fibres are shown, the last three fibres are non-zero dispersion shifted fibres from different manufacturers. The fibres are ordered with descending dispersion parameter. [1].

approximately $450m$ whereas the dispersion length of the SLA fibre is only $\sim 95m$. For a transform limited pulse the dispersion length can be regarded as the length at which the pulse have been broadened by some fixed factor, relative to the initial pulse width, dependent on the spectrum of the pulse. Comparing to the results presented in figure 2.1(a) the pulse should propagate about $\sim 900m$ in the TW-RS fibre before the FWHM pulse width would have broadened by a factor of 2.2 of the initial width, whereas in the SLA fibre the pulse should propagate only $\sim 190m$ to experience the same broadening. Hence a high dispersion leads to a rapid broadening.

2.2 Higher order dispersion

The effect of higher order dispersion is investigated in this section. The focus will be on the third and fourth order terms in the Taylor expansion of the wave number, $\beta(\omega)$ given in equation 2.4. The higher order terms are only of interest when the pulses becomes short, i.e the bandwidth of the pulses become sufficient large. The higher order terms affect the high frequency components more than the lower frequency components[1]. This can be seen from the the fact that the Taylor expansion of the wave number is an approximation to the real function in a small frequency bandwidth using polynomials as the base.

In figure 2.3 the sole effect of the third order term, which is proportional to β_3, is shown for both a Gaussian and a Sech pulse. The initial pulse width is the same as in figure 2.1. Due to the obvious difference in the appearance of the

---

[1] Since the frequencies are all measured relative to the center frequency the term high frequencies will throughout this thesis signify frequencies with a high numerical value, whereas low frequencies indicates the frequencies with a small numerical value. The sign of the frequencies will be signified by the term blue and red shifted frequencies, denoting positive and negative frequencies relatively.

(a) Gauss   (b) Sech
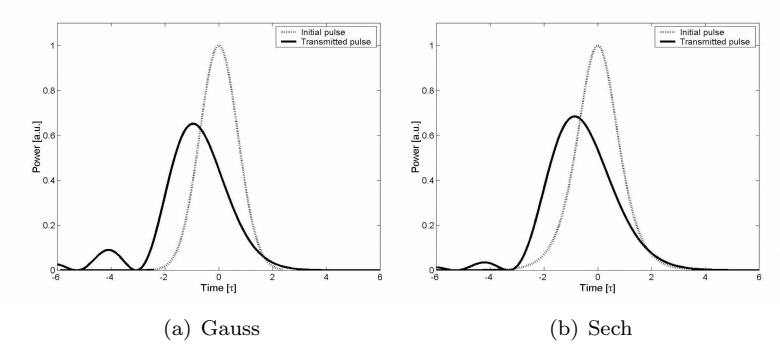
Fig. 2.3: Pulse distortion due to $\beta_3 > 0$ for $x^{(3)} = 4$. The evolution of the Gaussian pulse is shown in (a) and in (b) the Sech pulse evolution is shown.

pulse shapes the transmitted pulse has not been normalized. The time scales are the same but the length scale used is the dispersion length associated with the third order group velocity dispersion, equation 2.10. $x^{(3)}$ is thus defined as the ratio between the physical length, z, and the third order dispersion length, $L_D^{(3)}$.

$$(2.10) \quad L_D^{(3)} = \frac{T_0^3}{|\beta_3|}$$

It is seen that for both the Gaussian and Sech pulses the effect of the third order term is asymmetric. In this case where $x^{(3)} = 4$ it is seen that the leading edge of the pulses oscillate and that the peak is shifted towards the leading edge of the original pulse as well. This asymmetry is due to the odd phase shift introduced to the different frequency components by the third order terms. The actual phase shift is not what determines the pulse shape, however the frequency spectrum and the differences in the phase shifts of the different components, chirp, determine the pulse shape. In the linear case the pulse spectrum does not change and thus the only way of changing the pulse shape is to introduce a chirp. In the case of the calculations where $\beta_3 > 0$ the center frequency is moving faster than both the blue- and red-shifted components. Thus the energy is shifted towards the leading trail of the pulse, as can be seen by the shift of the peak. Furthermore this also explains the oscillations, i.e. the oscillations are a result of the beating between the blue- and red-shifted

components. In comparison the second order dispersion term with $\beta_2 > 0$ the blue-shifted components are moving faster than the red-shifted, which in this case also moves slower than the central components leading to a pulse broadening contrary to the pulse distortion of the third order dispersion or any odd numbered higher order terms.

(a) Gauss   (b) Sech
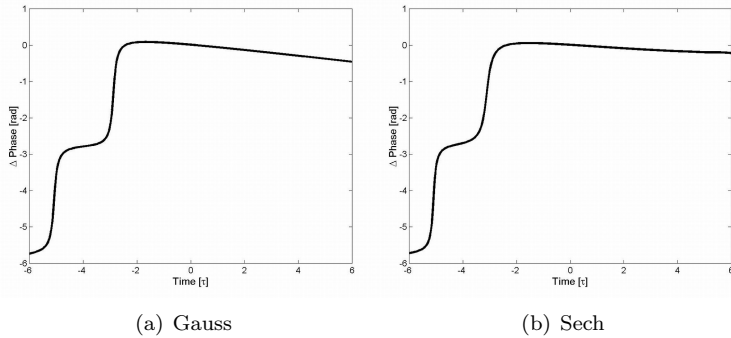
Fig. 2.4: Temporal variation of the phase shift due to β_3 for the pulses shown in figure 2.3. The case with the Gaussian pulse is shown in (a) and in (b) the phase shift of the Sech pulse is shown.

In figure 2.4 the temporal variation of the phase shifts are shown, again with the phase shift for the Gaussian pulse in figure 2.4(a) and the phase shift of the Sech pulse in figure 2.4(b). It is seen that for the leading edge there are some large variations in the phase whereas the phase is almost constant with a slight descent at the trailing edge, indicating that the central frequencies travel in the trailing edge whereas the high frequencies travel faster.

In figure 2.6 the phase shifts caused by the fourth order term are shown for the Gaussian (a) and the Sech (b) pulse. It is seen that the phase is very flat around $\tau = 0$ and that the sides are very steep; especially for the Sech pulse this behaviour of the phase is clear. As opposed to the asymmetrical phase and pulses of the third order term the phases of the fourth order terms are symmetrical. This symmetry translates to a symmetric pulse shape as seen in figure 2.5 where the pulses have been normalized to the peak power. The calculations shown for the fourth order dispersion term is done for a normalized length, $x^{(4)} = 6$, associated with β_4 in the same way as the second and third

order terms 2.11.

(2.11) $L_D^{(4)} = \dfrac{T_0^4}{|\beta_4|}$

The very flat central part of the phase shift indicates that the central spectral components are affected little by the fourth order dispersion. The symmetrical phase, which is equivalent to an even wave number, suggests that group velocity is odd. This corresponds to the fact that blue-shifted components travel slower than red shifted in the case $\beta_4 > 0$, which is equivalent with the effect of β_2 and other even numbered higher order dispersion terms.

(a) Gauss (b) Sech
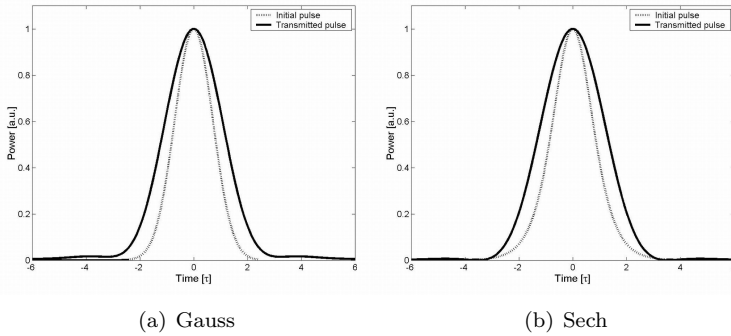
Fig. 2.5: Pulse broadening due to $\beta_4 > 0$ for $x^{(4)} = 6$. The transmitted pulse have been normalized to the peak power. The evolution of the Gaussian pulse is shown i (a) and in (b) the Sech pulse evolution is shown.

Even though the dispersion length associated with β_4, $L_D^{(4)}$, is three times larger than the dispersion length, L_D, the pulse widths in figure 2.5 are not as broad as the pulses in figure 2.1. The peak powers have been normalized to the peak power for direct comparison of the initial and transmitted pulse. For the Gaussian pulse the broadening of the FWHM pulse width due to β_4 is ~ 1.5, whereas the FWHM pulse of the Sech pulse is broadened a bit more with a broadening factor of ~ 1.6. Comparing these broadening factors with those due to β_2 where the FWHM pulse widths after propagation of only two dispersion lengths was broadened by a factor of 2.2 it seems as if β_4 is weaker than β_2. This is due to the fact that β_4 act more strongly on the high frequency

components than the low frequencies, which can be seen from the plot of the
phases 2.6. However the plateau seen on both the leading and trailing edges can
be quite detrimental for transmission systems since they degrade the quality of
the optical eye; the zero-level is increased. The one-level is decreased due to the
lower peak, which is not seen in figure 2.5 due to the normalization of the power.
The distortions of the third order terms are surely also very deterring for the
transmission system since both the change the position of the pulse with within
the time slot and also the oscillations disturb the neighboring bits and raises
the zero level. Of course the group velocity dispersion also degrades system
performance due to leakage of power into neighboring bits.

(a) Gauss   (b) Sech
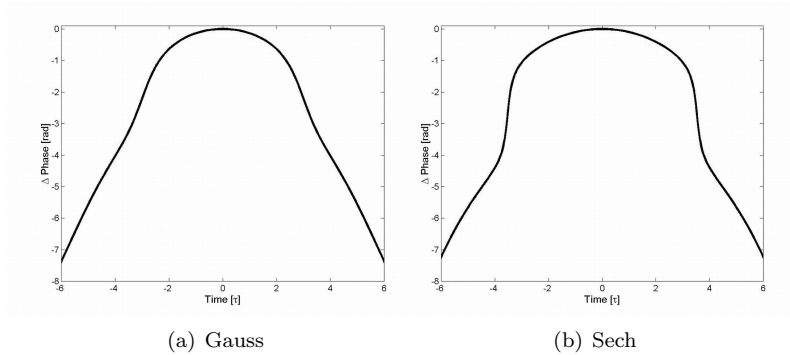
Fig. 2.6: Temporal variation of the phase shift due to β_4 for the pulses shown
in figure 2.5. The case with the Gaussian pulse is shown i (a) and in
(b) the phase shift of the Sech pulse is shown.

2.2.1   Dispersion slope

In table 2.2 the higher order group velocity dispersion parameters for the trans-
mission fibres given in table 2.1 is shown. The higher order group velocity
dispersion terms where calculated using the equations 2.12 and 2.13. The pa-
rameters were calculated from values given in table 2.1. In calculating the fourth
order dispersion parameter β_4 the curvature of the fibres were assumed zero.

$$(2.12) \quad \beta_3 = \frac{\lambda^3}{(2\pi c)^2}(2D + \lambda S)$$

(2.13) $\beta_4 = -\dfrac{\lambda^4}{(2\pi c)^3}(6D + 6\lambda S + \lambda^2 C)$

where C is the curvature of the dispersion parameter curve i.e. $C = \frac{d^2}{d\lambda^2}D$.

	Unit	SLA	SMF	TeraLight	TW-RS	E-LEAF
β_2	ps^2/km	-26	-22	-12	-5.8	-5.4
β_3	ps^3/km	0.14	0.13	0.11	0.083	0.15
β_4	ps^4/km	$-6 \cdot 10^{-8}$	$-5 \cdot 10^{-8}$	$-2 \cdot 10^{-8}$	$-1 \cdot 10^{-8}$	$-2 \cdot 10^{-8}$

Tab. 2.2: The higher order group velocity dispersion parameters at 1550nm for five different transmission fibres are shown. The fibres are ordered as in 2.1.

The slope, S, of the transmission fibres in table 2.1 were given to complete the dispersion data of the fibres. Equation 2.14 shows the definition of S. In the literature the practice of calling the dispersion slope a second order dispersion is widely spread, however as seen in equation 2.14 the slope depends also on the third order chromatic dispersion coefficient, β_3.

(2.14) $S = \dfrac{dD}{d\lambda} = \left(\dfrac{2\pi c}{\lambda^2}\right)^2 \left[\dfrac{\lambda}{\pi c}\beta_2 + \beta_3\right]$

The ratio, η, between the contribution of β_3 and β_2 to S is given in equation 2.15.

(2.15) $\eta = \dfrac{\pi c}{\lambda}\dfrac{\beta_3}{\beta_2}$

To investigate the relative weight of each of the group velocity dispersion terms in S, η for the wavelengths $\lambda = \{1520nm, 1550nm, 1620nm\}$ is calculated from equation 2.15 using the values in table 2.2. As seen in table 2.3 η is negative

λ	SLA	SMF	TeraLight	TW-RS	E-LEAF
$1520nm$	-3.5	-3.7	-6.7	-8.9	-17.0
$1550nm$	-3.4	-3.6	-6.6	-8.8	-16.7
$1620nm$	-3.3	-3.5	-6.3	-8.4	-16.0

Tab. 2.3: η for the different transmission fibres at the wavelengths $1520nm$, $1550nm$, $1620nm$.

for all the fibres due to the different signs of β_2 and β_3. Since $|\eta| > 1$ β_3 is

the main contributor to S in the wavelength range most common for optical communications—namely the C- and L-band. The role of β_2, however is to lower S due to the sign of β_2.

The question whether or not the higher order group velocity dispersion plays a vital role in transmission systems utilizing the fibres in table 2.1 remains. To clarify this question the data shown in table 2.2 are quite useful. As a first estimation the ratio of the higher order terms to β_2 could be used to determine if the higher order term has an influence on the non-linear Schrödinger equation 2.1. However as seen in the earlier discussion 2.2 the bandwidth, $\Delta\omega$, of the optical field has a strong influence of the pulse broadening i.e. the broader the bandwidth the more the higher order terms influence the transmission of the field. Since the pulse width $T_0 \sim \frac{1}{\Delta\omega}$ the dispersion lengths equations 2.6, 2.10, and 2.11 could be used to weigh the influence of the different terms against each other. Taking β_2 as the reference the ratio of the dispersion lengths is given in equation 2.16.

$$(2.16) \quad \rho^{(i)} = \frac{\beta_2}{\beta_i} T_0^{i-2} \qquad i = 3, 4, \ldots$$

where the counter i denotes whether ρ is evaluated with respect to β_3, β_4 or an even higher order. $\rho^{(4)} \approx 5 \cdot 10^9$ for a pulse width of 1.56ps. β_4 most definitely does not contribute to the propagation for any real fibre at transmission speeds at $160Gbit/s$. Thus β_4 is negligible for most practical cases below $160Gbit/s$.

T_0	SLA	SMF	TeraLight	TW-RS	E-LEAF
1.56ps	278	260	143	108	57
6.25ps	1113	1039	572	433	227
$\frac{\beta_3}{\beta_2}$ [fs]	5.6	6.0	11	14	28

Tab. 2.4: $\rho^{(3)}$ is calculated for two pulse widths corresponding to $160Gbit/s$ (upper row) and 40Gbit/s (lower row) assuming a duty cycle of 0.25. The lower row shows the pulse width, where the dispersion lengths are equal.

$\rho^{(3)}$ is evaluated in table 2.4 for 1.56ps and 6.25ps corresponding to $160Gbit/s$ and 40Gbit/s relatively, when a duty cycle of 0.25 is assumed. It is clearly seen that $L_D^{(3)}$ is very long compared to L_D for all the fibres when transmitting at 40Gbit/s leaving β_3 negligible when compared to β_2. Also at $160Gbit/s$ $L_D^{(3)}$ for most fibres is very long. It must be noted that these arguments only hold

if the system is limited by dispersion. For a dispersion compensated system without slope compensation the accumulated β_3 might have a greater influence. In the $160 Gbit/s$ case $L_D^{(3)} \approx 26km$ for both the SLA and the E-LEAF. With no slope compensation the accumulated β_3 would after only one $\sim 80km$ span correspond to $\sim 3L_D^{(3)}$. Assuming that the dispersion is compensated the accumulated effect of β_3 would cause some serious distortions to the pulses and cause penalties to the system performance.

To further illustrate the relations between β_2 and β_3 the pulse width at which $\rho^{(3)} = 1$ is shown on the third row of table 2.4. Thus the pulse should be in the order of $10fs$–$100fs$ if β_3 is going to affect the pulse propagation through the transmission fibre.

2.2.2 Constant β_2 fibres

In the previous section the influence of the higher order terms were discussed. In order to see if the higher order terms could be precluded by designing a fibre without higher order dispersion the possibility to design a fibre with constant β_2 has been investigated. Such a fiber might be interesting for high bitrate fiber based components.

The condition for a constant β_2 is simply that $\beta_3 = 0$ because β_3 is the derivative of β_2. From equation 2.12 it is seen that the condition $\beta_3 = 0$ is satisfied when equation 2.17 is satisfied.

$$(2.17) \quad \frac{dD}{d\lambda} = -\frac{2D}{\lambda}$$

This equation has the solution given in equation 2.18 where the condition $D_0 = D(\lambda_0)$ has been used.

$$(2.18) \quad D(\lambda) = D_0 \left(\frac{\lambda_0}{\lambda} \right)^2$$

Comparing with the definition of the dispersion parameter in equation 2.9 the solution to equation 2.17 given in equation 2.18 is not very surprising. The solution might as well have been deduced from equation 2.9 simply by requiring β_2 to be a constant. It is seen that the sign of S must be opposite of D for a constant β_2 fibre. This fact makes it quite difficult to realize a fibre with relative large anomalous dispersion ($D > 0$) where β_2 is constant. For fibres with normal dispersion this task of finding a design is much easier; the first dispersion compensating fibres actually had a positive slope while the dispersion was negative [28].

2.3   Chromatic dispersion compensation

In this section some basic considerations of dispersion compensation using op-
tical fibres with negative dispersion parameter is discussed. There exist a wide
variety of different dispersion compensating techniques. In this work the focus
has been on single mode dispersion compensating fibres i.e. optical fibres with
normal dispersion in the C-band which is in the wavelength range 1520nm–
1570nm.

For a system with $160Gbit/s$ transmission rate chromatic dispersion com-
pensation is a necessity. To illustrate this a transmission system at $160Gbit/s$
with a 0.25 duty cycle is considered. Using a time scale, τ, normalized with the
pulse width, a bit slot would be exactly four time units. As seen on figure 2.1
the FWHM pulse widths of both the Gaussian and the Sech pulses are approxi-
mately four time units, i.e. after transmission of only two dispersion lengths the
pulses begins to spread into the neighboring bit slots and thereby diminish sys-
tem performance. Taking the calculated dispersion lengths for the transmission
fibre in section 2.1.1 it is seen that transmission systems based on the non-zero
dispersion shifted fibres are limited to a few kilometers only, whereas the non
shifted fibres (SMF, SLA) would be limited to a few hundreds of meters if no
dispersion compensation is used. In practical systems the required transmission
lengths are much longer than just a few kilometers so dispersion compensation
is essential for the realization of $160Gbit/s$ transmission.
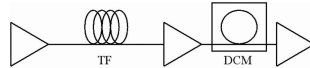
Fig. 2.7: A schematics of the basic deployment of dispersion compensating
          fibres. The transmission fibre is denoted TF and the DCM is the
          dispersion compensating module.

Figure 2.7 shows a basic schematics of how the dispersion compensating
fibres traditionally are deployed in transmission systems. Following the trans-
mission fibre and an amplifier the dispersion compensating module contains the
necessary length of dispersion compensating fibre needed to compensate the
dispersion arising from the transmission fibre [1].

The condition for full dispersion compensation is shown in appendix B using
a chirped Gaussian approach. Due to linearity the total dispersion, D_T, of a
dispersion compensated span is given in equation 2.19

$$(2.19)\quad D_T = D_{TF}L_{TF} + D_{DCM} = D_{TF}L_{TF} + D_{DCF}L_{DCF}$$

where D_{TF} id the dispersion parameter for the transmission fibre with length, L_{TF} and the total dispersion of the dispersion compensating module is $D_{DCM} = D_{DCF}L_{DCF}$. In practical transmission systems it is often preferred not to compensate the dispersion completely leaving some residual dispersion after each link. The dispersion compensating ratio, CR, given in equation 2.20 is thus a convenient parameter to establish the degree of dispersion compensation.

$$(2.20) \quad CR = 1 - \frac{D_T}{D_{TF}L_{TF}} = -\frac{D_{DCM}}{D_{TF}L_{TF}}$$

The system is said to be under compensated if $0 < CR < 1$ and over compensated if $CR > 1$. CR is however often chosen to be in the range $0.9 \leq CR \leq 1.1$, [29]. The required length of the dispersion compensating module is thus given in equation 2.21.

$$(2.21) \quad L_{DCF} = \frac{D_{DCM}}{D_{DCF}} = -CR\frac{D_{TF}L_{TF}}{D_{DCF}}$$

Neglecting splice loss the insertion loss, IL, of the DCM can be expressed in terms of the total dispersion of the module.

$$(2.22) \quad IL = \alpha_{DCF}L_{DCF} = D_{DCM}\frac{\alpha_{DCF}}{D_{DCF}} = \frac{D_{DCM}}{FOM}$$

where the power figure of merit, $FOM = \frac{D_{DCF}}{\alpha_{DCF}}$, of the DCF is introduced. IL can be minimized by maximizing the FOM [30]. Thus a dispersion compensating fibre with a numerical high dispersion parameter will yield a high FOM A figure of merit including the non-linear coefficient has been suggested [31] for the DCF. [32, 28] have both argued that the power FOM is sufficient as a figure of merit for the dispersion compensating module. The non-linear FOM actually varies monotonous with the power FOM due to the fact that the non-linear coefficient depends on the dispersion parameter through the effective area of the DCF.

The fundamental mode of single mode fibres actually is two fold degenerate due to the polarization of the optical field, which have two orthogonal states. This degeneracy only holds for a perfectly circular geometry of a fibre with no applied stresses or strains. The fibre geometry in fibres are generally not circular, due to inhomogenities in fabrication. The imperfect geometry of the fibres causes the two polarization modes to split up causing pulse broadening due to the differential group delay, $\Delta\tau_g$, of the two polarization modes. $\Delta\tau_g$ scales with the square root of the fiber length [33]. The polarization mode

dispersion parameter, PMD, is thus $\Delta\tau_g$ normalized to the square root of the fibre length. For a dispersion compensating module the total differential group delay is found by using equation 2.21.

$$(2.23)\quad \Delta\tau_{g,DCM} = PMD\sqrt{L_{DCF}} = \frac{PMD}{\sqrt{|D_{DCF}|}}\sqrt{|D_{DCM}|}$$

For dispersion compensating modules it is thus useful to express the PMD in terms of D_{DCF} and thus defining a figure of merit for PMD.

$$(2.24)\quad FOM_{PMD} = \frac{PMD}{\sqrt{|D_{DCF}|}}$$

The lower FOM_{PMD} the lower the total differential group delay of the dispersion compensating module[2]. A high fibre numerical dispersion lowers $\Delta\tau_g$ just as it lowers the insertion loss of the module which is beneficial for most cases. As such there is no need for a figure of merit for the differential group delay since it would follow the power FOM, however FOM_{PMD} is a nice design parameter since it allows a direct estimation of the module differential group delay from the desired module dispersion. Reducing the differential group delay of the module is not only achieved by maximizing the numerical value of the dispersion parameter but also reducing the fibre PMD through improved fabrication is important [34].

The accumulated slope of a dispersion compensated span reduces the optical bandwidth applicable to a wavelength division multiplexing system [35]. Thus simultaneous dispersion and slope compensation is required in the modern systems. The requirement for slope compensation can be derived from equation 2.25, where the total accumulated slope, S_T, of a single dispersion compensated span is shown.

$$(2.25)\quad S_T = \left(\frac{S_{TF}}{D_{TF}} - CR\frac{S_{DCF}}{D_{DCF}}\right)D_{TF}L_{TF} = (RDS_{TF} - CR \cdot RDS_{DCF})D_{TF}L_{TF}$$

where the relative dispersion slope, $RDS = \frac{S}{D}$, has been introduced. The RDS is well suited as a design target parameter for dispersion compensation fibres with simultaneous slope compensation. The total accumulated slope is zero

---

[2] The usual use of figure of merits is that a higher figure merit is good, however in the case with FOM_{PMD} a low value is better. This has been chosen so since a low module PMD is favored.

when the slope compensation ratio, SCR, which is defined in equation 2.26, equals CR, i.e. $SCR = CR$.

$$(2.26) \quad SCR = \frac{RDS_{TF}}{RDS_{DCF}}$$

For over compensated systems RDS_{DCF} must be smaller than RDS_{TF} if the slope has to be compensated perfectly. For the case where $CR = SCR = 1$ the dispersion and slope are simultaneously perfect compensated. For the non zero-dispersion shifted fibres in table 2.1 the RDS values are relatively high, especially the E-LEAF with an $RDS = 0.02nm^{-1}$ at $1550nm$ requires high slope dispersion compensating fibres. However for most single wavelength systems at $40Gbit/s$ or below slope compensation is not as crucial as dispersion compensation, due to the fact that β_3 does not have a great impact on transmission. However for WDM purposes the bandwidth needed ($\sim 50nm$) is often much larger than the bandwidth of the single channel. Thus slope compensation is important in WDM systems to ensure that the accumulated numerical dispersion is kept below some threshold value in the bandwidth of the WDM systems and not to mitigate the effects of third order dispersion in each of the WDM channels. However for optical time division multiplexed systems operating at bit rates of $160Gbit/s$ or higher the accumulated slope might impair the system performance if not compensated and the role of slope compensation is thus to mitigate the effect of β_3. The requirements for the dispersion slope compensation ratio must be established in order to avoid the impact of accumulated slope. From equations 2.20 and 2.25 the RDS_{DCF} can be found.

$$(2.27) \quad RDS_{DCF} = \frac{D_{TF}L_{TF}RDS_{TF} - S_T}{D_{TF}L_{TF} - D_T}$$

In order to estimate the requirements of the RDS for a dispersion compensating fibre for the TW-RS the dispersion and slope tolerance has to be established. As an estimation of the dispersion tolerance the total dispersion corresponding to one dispersion length is taken as the upper limit of the allowed residual dispersion, since it is seen in figure 2.1 that the FWHM pulse width is comparable to the time slot after only two dispersion lengths. Equivalently the total slope corresponding to one third order dispersion length is taken as the slope tolerance. Since the dispersion length of a $1.56ps$ pulse propagating in the TW-RS is $\sim 420m$ at $1550nm$ the total residual dispersion is $\sim 2ps/nm$, giving a dispersion tolerance of $\pm 2ps/nm$. Further from the data in table 2.4 $L_D^{(3)}$ can be found from the dispersion length. $L_D^{(3)}$ is found to be $45.7km$

resulting in an estimated slope tolerance of $\pm 2ps/nm^2$. For an $80km$ span equation 2.27, using the above mentioned limits, yields the RDS_{DCF} interval: $0.0044nm^{-1} < RDS_{DCF} < 0.0156nm^{-1}$ for which the effect of β_3 is negligible when the dispersion has been compensated. It is seen that for $160Gbit/s$ transmission the requirements of the slope compensation is not as strict as the requirements for the dispersion compensation. Since $99, 4\% < CR < 1.006\%$ and $0.44 < SCR < 1.6$ this is due to the fact that the $\rho^{(3)} \gg 1$. Although the requirements of the RDS of the DCF is somewhat relaxed compared to the dispersion compensation ratio a SCR around 1 is often preferred due to the larger bandwidth available for WDM transmission.

2.3.1 Dispersion managed spans

In recent years there has been a shift in the way dispersion compensation fibres are deployed. This shift has in particular been pioneered by the under sea industry [32]. Dispersion managed spans are the new alternative method of deploying DCFs. In dispersion managed spans the dispersion fiber is used as a part of the span as shown in figure 2.8. The use of the dispersion compensation fibre as a transmission fibre calls for a different set of requirements for the optical properties of the fibre compared to the fibre used in modules. The dispersion of the fibres used in modules should be as high numerically as possible in order to decrease the insertion loss, polarization mode dispersion and the bulk of the modules. Using the dispersion compensating fibre as a part of the transmission obviates the concept of dispersion compensating fibres since both fibres in the span are used as a transmission fibre and acts as the dispersion compensating fibre for its counterpart i.e. both fibres could in fact be regarded as the dispersion compensating fibre. A conveyance from the traditional usage of terms in which the negative dispersion fibre is the dispersion compensating fibre could be adopted. This terminology is, however, not very precise. Instead a new terminology, where the sign of the dispersion distinguishes the fibre apart, is used in the remainder of this thesis when dispersion managed spans are considered. The shown dispersion map is not universal for dispersion managed spans and
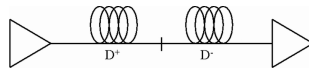
Fig. 2.8: Schematics of a dispersion managed span.

others not shown exist and are used. For dispersion managed spans it makes no sense to speak of insertion loss of the D^- fibre since it is a part of the

transmission span. However an average span attenuation coefficient can be found as shown in equation 2.28.

$$(2.28) \quad \alpha_{span} = \alpha^+ + (\alpha^- - \alpha^+) \left(1 - \frac{D^-}{CR \cdot D^+}\right)$$

The length ratio of the fiber segments, the dispersion managed span is composed of, are mutually dependent on the dispersion parameters of the fibres and the dispersion compensation ratio. Furthermore the span length, L_{span}, determines the actual length of each segment as seen in equations 2.29 and 2.30

$$(2.29) \qquad L^+ = \left(1 - \frac{CR \cdot D^+}{D^-}\right)^{-1} L_{span}$$

$$(2.30) \qquad L^- = \left(1 - \frac{D^-}{CR \cdot D^+}\right)^{-1} L_{span}$$

where the superscripts $^+$ and $^-$ denotes the positive and negative dispersion fibre.

2.4   Fibre design

In this section a brief discussion of dispersion compensation module design is given. The triple clad index profile shown in figure 2.9 was the base for the work on fibre design. An elaborate discussion on the design issues for dispersion compensating fibres have already been discussed in [28, 32] The triple clad index profile consist of a core, which for dispersion compensating fibres has a high index due to a high Germanium doping. There are three cladding layers. The layer close to the core is called the trench and the neighboring layer is the ring since it forms a ring, when observed at a cross section perpendicular to the fibre length. The outermost cladding layer is by far the thickest layer of the fibre and corresponds to the cladding of a step index fibre. By adjusting the relative radii and indices of the different layers the dispersion of the fibre is changed.

The dispersion of a fibre is comprised of three terms [36], material dispersion, wave guide dispersion and profile dispersion. In dispersion compensation fibres the latter two are dominant, whereas the dispersion of non shifted fibres are dominated by material dispersion [28]. Typical dispersion and RDS curves are shown figure 2.10(a) and (b) relatively. The curves are simulation data obtained by the use of the in-house design tool of OFS Fitel. The in-house design tool
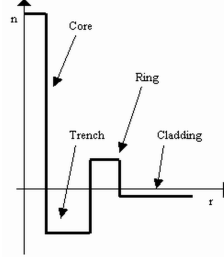
Fig. 2.9: The triple clad index profile used in the DCF design presented in this thesis.

(a) Dispersion

(b) *RDS*
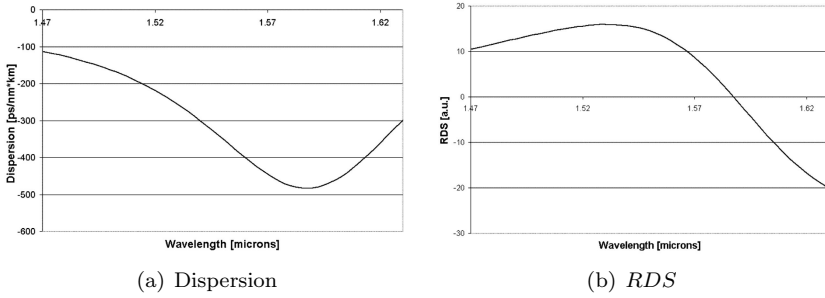
Fig. 2.10: The typical dispersion (a) and *RDS* (b) for the triple clad index profile. The figures are simulated using the in-house design tool available at OFS Fitel Denmark.

gives the wavelength in μm. In the dispersion curve shown in figure 2.10(a) it is seen that the dispersion has a minimum point. Comparing with the RDS curve shown in figure 2.10(b) it is seen that $RDS = 0$ at the wavelength where the dispersion is minimal due to the fact the the slope is zero at the extremum point. However for practical design the descending part of the dispersion curve is used, since above the minimum point the macro bending loss of the fibre becomes a severe limiting factor. However it is easily seen that the RDS curve has a maximum point at a wavelength given by the relation in equation 2.31.

$$(2.31) \quad S^2 = C \cdot D$$

From equation 2.31 it is seen that the maximum value occurs at a point where

the dispersion curve must be concave since the dispersion is negative i.e. the maximum point lies at a wavelength lower than the inflexion point. At a small part of the dispersion curve around the inflexion point the dispersion curve is at it's most linear part and this is the key to a proper slope compensation. In section 2.3 the condition for slope compensation was discussed in term of RDS and SCR. It was seen that for $SCR = 1$ the RDS of the transmission fibre and dispersion compensating fibre should be equal, in order to provide full dispersion and slope compensation. In order to have a broad-band slope compensation it is therefore optimal if the fibres could be signed so that the RDS curves for the fibres would be coincident. However this is not possible, due to the fact that the dispersion of most transmission fibres are very linear in the wavelength range of interest, whereas the dispersion compensating fibre does have some curvature.

In practical fibres the RDS curves of the fibres would intersect in one point or simply do not intersect each other at any points. The latter case correspond to the case where $SCR > 1$ since the RDS of the transmission fibre must be greater than the RDS of the DCF. In the case where the RDS curves intersect in one point the residual dispersion would be paraboloid around the intersection point as seen in figure 2.11(a). Figure 2.11(b) shows actual RDS curves for realized fibres. The fibre EHS (see 2.4.1) is a dispersion compensating fibre which provides full slope compensation of the non-zero dispersion shifted fibre TW-RS. The RDS of the EHS is shown with the full line whereas the TW-RS RDS is depicted with the dotted line. The broadest slope compensated bandwidth obtainable if the fibres are designed so that the RDS curves intersect at the DCF inflexion point, provided that only one intersection point is obtained in the wavelength range of interest.

To realize an even broader slope compensated range a design must be found where the RDS curves intersect twice within a relative small bandwidth as seen in figure 2.12, where the slope compensated bandwidth has almost doubled compared to the residual dispersion depicted in figure 2.11(a). In figure 2.12(a) it is seen that the dispersion varies less around the local maximum then around the local minimum. This is a result of the intersection points of the RDS curves seen in figure 2.12(b). It can be seen that the intersection point corresponding to the local maximum of the residual dispersion is very close to the inflexion point of the DCF dispersion curve i.e. the maximum of the RDS curve. The intersection point corresponding to the minimum residual dispersion is farther away from the inflexion point and thus varies more. Hence the broadest slope compensated bandwidth will be obtained by a DCF with a RDS curve that intersects the corresponding RDS curve of the transmission fibre twice around the inflexion point. Further a DCF design where the maximum of the RDS

(a) Dispersion

(b) *RDS*
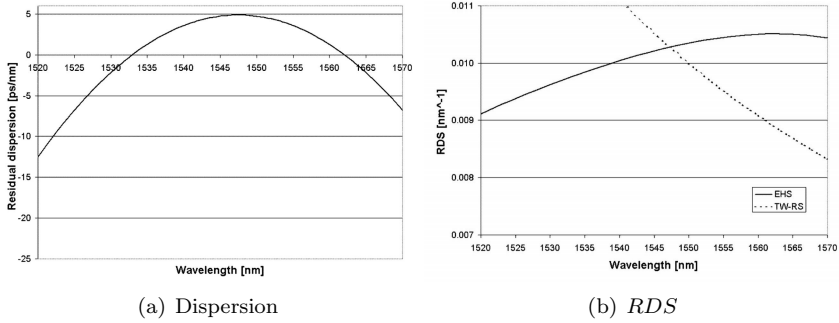
Fig. 2.11: The measured residual dispersion (a) and *RDS* curves (b) for an actual span of a non-zero dispersion shifted fibre and a matching dispersion compensating fibre.

(a) Dispersion

(b) *RDS*
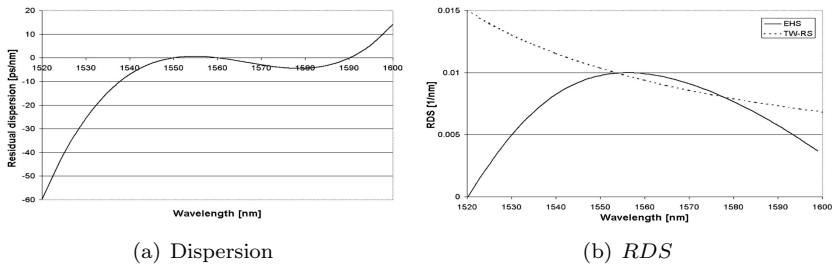
Fig. 2.12: The measured residual dispersion (a) and *RDS* curves (b) for an actual span of a non-zero dispersion shifted fibre and a matching dispersion compensating fibre.

curve is very broad also allows a broad slope compensation bandwidth.

In the preparation of the dispersion compensating module the best wavelength to match the dispersion of the module is to use the midpoint wavelength of the intersection of the *RDS* curves.

2.4.1   EHS—The fibre

The fiber data for the first realized extra high slope (EHS) module [7] is given in table 2.5. The fibre is a slope compensating fibre designed to match the non-

zero dispersion shifted fibre TW-RS in the C-band which in this work is defined to be the wavelength range $1530nm$–$1565nm$. As seen the RDS of the fibre at $1550nm$ is $0.0094nm^{-1}$ which provides a very well slope compensation ratio of ~ 1 for the TW-RS. However for the E-leaf the slope compensation ratio is ~ 0.5 which is expected to be in the lower bound of the slope compensation needed for transmission at rates of $160Gbit/s$. The PMD figure of merit is also very low, only $0.0048\sqrt{ps \cdot nm}$. The total differential group delay of the a module can be estimated from FOM_{PMD} by multiplication of the square root of the target dispersion of the module. Thus for a module for $80km$ of TW-RS the total differential group delay would be estimated to only $0.09ps$. The FOM

α	A_{eff}	D	RDS	FOM	FOM_{PMD}
$[dB/km]$	$[\mu m^2]$	$[ps/(nm \cdot km)]$	$[nm^{-1}]$	$[ps/(nm \cdot dB)]$	$[\sqrt{ps \cdot nm}]$
0.55	15	-144	0.0094	261	0.0048

Tab. 2.5: Fibre data at $1550nm$ for the fibre used in the first EHS dispersion compensating module.

of the fibre is $261ps/(nm \cdot dB)$. The effective area $A_{eff} = 15\mu m^2$ giving rise to a non-linear coefficient, $C_{NL} = \frac{A_{eff}}{n_2}$ which is considerable larger than the TW-RS. The non-linear coefficient of the EHS fibre is measured to $1.8 \cdot 10^{-9}W^{-1}$ whereas a typical value for the TW-RS is $4.3 \cdot 10^{-10}W^{-1}$, the TW-RS non-linear coefficient has been measured on one fibre however is comparable with the values obtained in [37]. However the ratio between the non-linear parameter and $|\beta_2|$ is $9.8 \cdot 10^{-12}W^{-1}ps^{-2}$ for EHS and $75 \cdot 10^{-12}W^{-1}ps^{-2}$ for the TW-RS indicating that the nonlinear term in the Schrödinger equation will be more significant for the TW-RS fibre than the EHS at the same power level into the fibres.

The EHS fibre is also suitable to compensate the E-LEAF in the L-band since the RDS of the E-leaf at $1590nm$ is in the order of $0.011nm^{-1}$. Figure 2.13 shows the RDS curve of an EHS fibre, it is seen that the RDS at $1590nm$ is $0.0095nm^{-1}$ giving a $SCR = 1.16$. In figure 2.13 the RDS curve is shown for both the EHS and the transmission fiber. The full line is the RDS of the EHS and the dotted lines are the transmission fibre RDS. The line which intersects with the full line corresponds to the TW-RS fibre. It is seen that the residual curve resulting from a link consisting of the depicted EHS fibre and the TW-RS fibre will have a parabolic shape around the intersection wavelength. For a link with the E-LEAF in the L-band monotonically increasing residual dispersion with a low slope will be the result due to the incomplete slope match.

EHS fibres which provide 100% slope compensation for E-leaf in the L-band
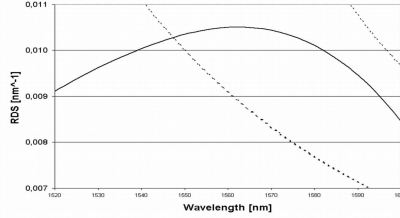
Fig. 2.13: The RDS of an EHS (full line), TW-RS (dashed line), and E-LEAF
        (dotted curve).

has been produced . Furthermore a new fibre developed by colleagues at OFS
Fitel Denmark which provide full slope compensation of the E-LEAF in the C-
band has been realized. Thus slope compensation is available for all transmission
fibres given in table 2.1.

2.4.2   EHS—Dispersion compensating module

In this section the results from the first slope matched dispersion compensating
module for TW-RS will be presented. The module was made from the fibre
shown in table 2.5. The fibre was wound on a spool with dimensions $40mm \times$
$(165mm^{\emptyset}/140mm^{\emptyset})$, where the inner diameter of the spool was $140mm^{\emptyset}$. At
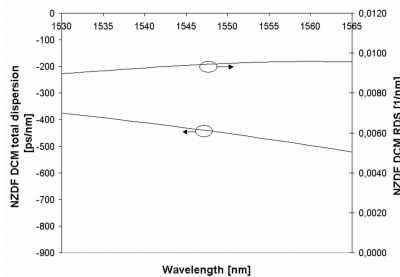
Fig. 2.14: The total dispersion and RDS of the first dispersion compensating
        module which provides full slope compensation of the TW-RS.

$1550nm$ the total dispersion of the module was $-452ps/nm$ and the $RDS =$
$0.0095nm^{-1}$. The total differential group delay of the module was $0.08ps$ which
corresponds well to the estimated value of $0.1ps$, which is calculated from the

total dispersion and the FOM_{PMD} given in table 2.5. The deviation could be due to local variations of the fibre and the changed stresses and strains on the fibre during the the process of winding the fibre onto the module spool. However the FOM_{PMD} gives a good estimation of the differential group delay despite of the changing environment of the fibre.

The loss of the module is shown in figure 2.15 along with the total fibre attenuation of the fibre used in the module. The discrepancy of the two curves is due to splice loss. At $1550nm$ the splice loss is less than $1dB$. The insertion loss of the module including splice losses varies $\pm0.55dB$ in the C-band.
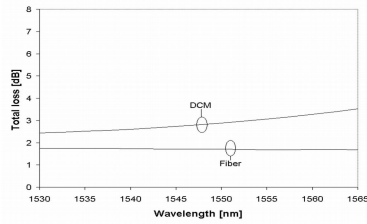
Fig. 2.15: The module insertion loss and fibre loss.

The measured residual dispersion of a span consisting of the EHS module and $96km$ of TW-RS with a dispersion of $4.8ps/(nm \cdot km)$ is shown in figure 2.16. The slope of the TW-RS fibre was $0.44ps/(nm^2 \cdot km)$. It is seen that the residual dispersion in the C-band only varies $\pm0.4ps/(nm \cdot km)$ when the residual dispersion has been normalized to the fibre length.
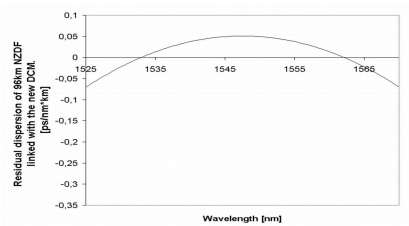
Fig. 2.16: The residual dispersion of the EHS module.

2.5   Measuring chromatic dispersion

As seen in section 2.3 the relative dispersion slope, RDS, is a very good design
target parameter. However measuring the dispersion slope should be done quite
accurately when slope compensation has to be taken into account as is the case
for OTDM systems with transmission rates of $160Gbit/s$ and above. WDM
systems at even lower transmission rates starting from 10Gbit/s also requires
slope compensation in order to utilize a large bandwidth up to $80nm$.

An investigation of the accuracy to which the slope of the dispersion com-
pensating fibres where measured at OFS Fitel Denmark has been performed
and the results are presented here. The dispersion of the fibres are measured
using a commercial device. The device uses the modulation phase shift method
[38] to determine the group delay at different wavelengths. The dispersion is
thus the derivative of the obtained curve. At OFS Fitel Denmark two gener-
ations of the device exist. In the first generation the transmitter consist of a
LED and a monochromator. This device measures rapidly, however without the
accuracy needed for an accurate measurement of the dispersion slope due to
the bandwidth of the monochromator. The second generation device measures
slower, however has a much better definition of the wavelength since a tunable
laser with a smaller bandwidth than the monochromator is used in conjunction
with a wavemeter, that determines the wavelength very accurately. The possible
wavelength range of the tunable laser is $1510nm$–$1620nm$[3]. In order to remove
the effect of noise on the derivation of the measured data the group delay curve
is traditionally fitted to a polynomial or an N-term Sellmeier function defined
in equation 2.32. The slope is the second derivative of the group delay, $\Delta\tau$.

$$(2.32)\ \ \Gamma(\lambda) = a_0 + \sum_{n=1}^{(N-1)/2} a_{2n-3}\lambda^{2n-3} + a_{-(2n-3)}\lambda^{-(2n-3)} \qquad N = 3, 5, 7, \ldots$$

The Sellmeier fitting functions up to 5-terms are traditionally used widely in
the industry although no physical arguments for choosing these functions as
fitting functions exist. The material refractive index can be expressed by an
expression much similar to equation 2.32, however the dispersion of dispersion
compensating fibres are determined mainly by the waveguide dispersion and
profile dispersion, and not by the material dispersion, ruling out the physical
argument for choosing the Sellmeier functions as fitting functions.

---

[3] A newer device has been setup at OFS Fitel Denamrk using two different tunable lasers
giving a much broader bandwidth covering wavelengths below $1510nm$.

The dispersion of a TW-RS and EHS link has been measured in order to investigate how the raw data from the dispersion measurements should be fitted. The dispersion of each of the TW-RS and the EHS where measured separately. The dispersion of the link could then be calculated from the measured fibre dispersions. The residual dispersion of the link was also measured in order to validate the different fitting schemes applied to the measured fibre data.

The measured data set is a combination of the true group delay and measurement errors. The errors vary much more rapid than the true group delay function. The fitting procedure should thus be regarded as a filtering process, where a low pass filter is applied to the raw data, allowing the true form of the group delay to pass. If the bandwidth of the filter is too large the noise is not filtered out efficiently. However if the bandwidth of the filter is too small the signal is not allowed to pass through the filter and some information is lost. The issue of determining the fitting functions and the fitting order is addressed in the following sections.

2.5.1 Fitting function

In this section an investigation of the most appropriate fitting function is carried out. The functions compared are the Sellmeier functions, S_n, and ordinary polynomials, P_n. Traditionally polynomials up to the fourth degree and 5-term Sellmeier functions has been used in the fitting procedure. The circumstances for which fits using the two different fitting functions provide reliable estimations of the group delay is investigated. Figure 2.17 shows the measured group delay
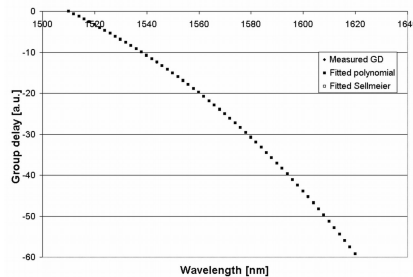
Fig. 2.17: The group delay curves of a fit to a fourth order polynomial and a 5-term Sellmeier to the same set of raw data is shown.

of an EHS fibre, when the raw data has been fitted directly to a polynomial of fourth degree and a 5-term Sellmeier function. The filled circles are the

measured raw data. The squares are the fitted data, where the filled squares
are the fitted group delay resulting from a fourth order fit. The 5-term Sellmeier
fit is the clear squares. As seen the group delay resulting from the fits are almost
identical. By inspection it seems that these fitting functions and fitting orders
are sufficient and give a reliable estimation of the true behaviour of the group
delay. Equation 2.33 shows how to derive the dispersion, D_m from the fitted
group delay, $\Delta\tau$ data.

$$(2.33) \quad D_m = \frac{d\Delta\tau(\lambda)}{d\lambda}$$

The unit on the ordinate in figure 2.17 is actually $[ns]$ the arbitrary unit shown
on the axis label illustrates that the measured group delay data are not the true
group delay since the first point is arbitrarily chosen to be zero.

However as seen in figure 2.18 where the same symbols as in figure 2.17
has been used to distinct between the polynomial and the Sellmeier fits. There
is a small but significant difference in the dispersion curves obtained from the
fits used in figure 2.17. Still it seems that both functions are applicable for
the fitting procedure. In figure 2.19 the relative dispersion slope derived from
the fitted group delay is shown. The RDS reveals that the two fits performed
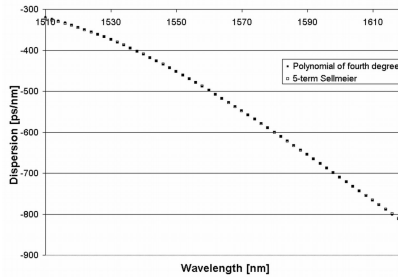
Fig. 2.18: The dispersion curves of a fit to a fourth order polynomial and a
5-term Sellmeier to the same set of raw data is shown.

do not yield a consistent measurement of the slope, due to the deviant RDS
curves. Since the midpoint of the wavelength range used in the measurement
is $1565nm$ the curves in figure 2.19 should be consistent at least around the
midpoint if the fits are accurate. The problem becomes clear when the squared
residuals are examined. The squared residuals for the polynomial fit and the
Sellmeier fit are shown in figure 2.20. The full line is the squared residuals of
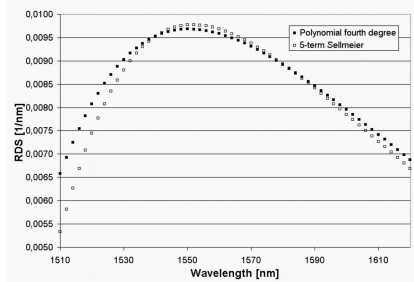
Fig. 2.19: The relative dispersion slope of a fit to a fourth order polynomial
           and a 5-term Sellmeier is shown.

the polynomial and the dotted line corresponds to the Sellmeier fit. Both of the
curves exhibit some slow variations indicating that the bandwidth of the fit is
not high enough. Apart from determining the apropriate fitting function it is
also of paramount importance to establish the correct fitting order. If the fitting
order is too low the fitted function is not a good estimate of the real function
of interest, however if the fitting order is too high the noise is included and the
fit turns into an interpolation of the measured points.
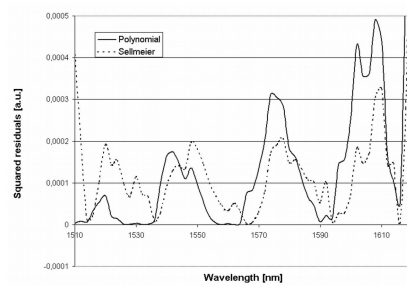
Fig. 2.20: The squared residuals of a fit to a fourth order polynomial and a
           5-term Sellmeier is shown.

2.5.2   Fitting range

Another way of improving the accuracy of the fit is to eliminate possible numer-
ical errors. The effect of re-scaling the wavelength from the $1510nm$–$1620nm$
range to the range $-1 < x < 1$ has been examined. The transformation into

the re-scaled abscissa is given in equation 2.34.

$$(2.34) \quad x = \frac{\lambda - \lambda_- + \lambda - \lambda_+}{\lambda_+ - \lambda_-}$$

where λ_+, λ_- is the upper and lower bound of the wavelength range of the measurement. The dispersion and the slope can thus be determined from the fits using the re-scaled abscissa, as shown in equations 2.35 and 2.36.

$$(2.35) \quad D_m = \frac{d\Delta\tau(x)}{d\lambda} = \frac{dx}{d\lambda}\frac{d\Delta\tau(x)}{dx} = c \cdot \frac{d\Delta\tau(x)}{dx}$$

$$(2.36) \quad S_m = c^2 \cdot \frac{d^2\Delta\tau(x)}{dx^2}$$

where $c = (\lambda_+ - \lambda_-)^{-1}$. Since the Sellmeier functions cannot be re-scaled by the new scale in equation 2.34 the fits using the Sellmeier functions are not re-scaled. The polynomial fit however is re-scaled, and as shown in figure 2.21. The RDS curves for the fourth order fits are with and without the re-scaling of the abscissa. The full line is the re-scaled RDS and the filled squares are the fit using the raw abscissa. There is a clear difference in the curves. However to establish whether the re-scaling has improved the fit or not further investigation is needed. A series of fits is performed with and without re-scaling in order to
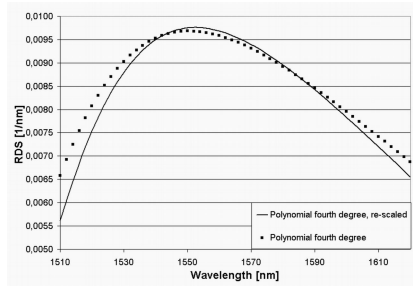
Fig. 2.21: The dispersion curves of a fit to a fourth order polynomial and a 5-term Sellmeier is shown.

test the influence of the re-scaling. Further this series is used to determine the optimum fitting order. The fitting order ranges from one to ten in the series of fits. A series of fits are also performed for the Sellmeier functions—the highest order is the 11-term Sellmeier. The sum of squared residuals, SSR, of each of the fits where calculated and plotted in figure 2.22. It must be noted that
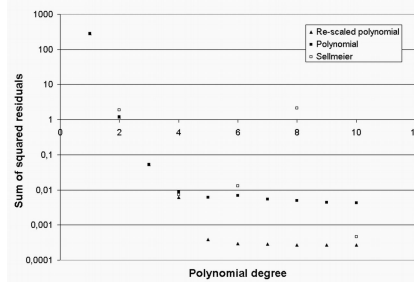
Fig. 2.22: The sum of squared residuals as the function of fitting order is shown
for the Sellmeier fits and the polynomials fit with and without re-
scaling of the abscissa.

minimizing the sum of squared residuals does not necessarily mean that the
optimum fitting order is found. In figure 2.22 the filled triangles represent the
sum of squared residuals of the fit using the re-scaled abscissa, the filled squares
are the fit without re-scaling and the empty squares are the Sellmeier fits. The
Sellmeier fits are only given at even polynomial order, n. The number of terms,
N, in the Sellmeier fit is determined from the polynomial order given in figure
2.22 by the following relation, $N = n + 1$. The ordinate in figure 2.22 is plotted
on a logarithmic scale. The sum of squared residuals for the polynomial fits
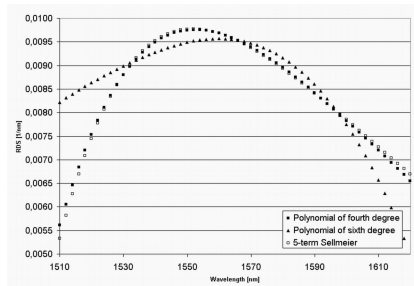
Fig. 2.23: The RDS calculated from a fourth and six order fit and a 5-term
Sellmeier is shown. The polynomials fits have both been re-scaled.

are high at the low fitting orders and decreases with increasing fitting order
until a low plateau is reached. It seen that as the fitting order is increased the
squared sum of residuals is decreased as an indication of a better fit, however,

as the fitting order is increased even further the sum of squared residuals does not keep decreasing but levels out. This occurs because no more information can be extracted from the raw data by increasing the fitting order, thus the fitting order at which the squared sum of residuals levels out can be taken as the optimum fitting order. In figure 2.23 it is seen that the polynomial fit with the original abscissa saturate at a fitting order of four or five, where the re-scaled fit saturate at an even higher fitting order of six. It is also seen that the sum of squared residuals levels out at a lower level for the re-scaled fit. This indicates that re-scaling improves the accuracy of the fit, which might be due to the finite numerical precision of the computer. The numerical errors in the calculation leads to the higher level of the plateau in the fit using the original scale. Thus it is seen that the optimum fitting order when using the polynomials is six, and that re-scaling increases the accuracy of the measurement significantly. The sum of squared residuals of the Sellmeier fit does not yield a clear answer to the optimum number of term in the fits since no clear plateau is found. This might be due to the fact that the terms in equation 2.32 do not form a complete set of orthogonal base, whereas the polynomials do.

In figure 2.23 the *RDS* curve obtained from a fourth and sixth order fit along with a 5-term Sellmeier fit, the re-scaled abscissa is used in the polynomial fits. The polynomial fits are shown with the filled symbols and the clear square is the 5-term Sellmeier. The sixth order polynomial fit is represented by the triangles. It is seen that the RDS of the sixth order fit and the 5-term Sellmeier are fairly coinciding, however, a small difference can be seen, It seems like the 5-term Sellmeier oscillates around the sixth order fit indicting that the fit does not provide a full description of the measured group delay. In figure 2.24 the residual
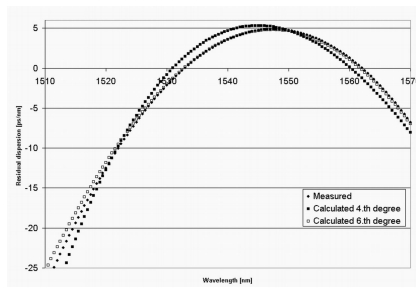
Fig. 2.24: The residual dispersion of a compensated span of TW-RS and EHS is shown. The measured dispersion is compared with the calculation of the residual dispersion from the measured fibre dispersion data.

dispersion of a TW-RS and EHS link is shown. The filled circles represent the residual dispersion of the link, where the link dispersion has been measured directly, by concatenating the fibres in the measurement setup. The squares are the residual dispersion resulting from the measured fibre dispersion, using the re-scaled fourth and sixth order fits. A remarkable resemblance between the sixth order fit and the measured link dispersion is obtained, whereas the fourth order fit does not fit very well to the measured link dispersion. The better performance of the sixth order fit than the fourth order fit is expected from the previous discussion. It is seen that in order to manufacture dispersion compensating for systems with transmission rates at $160Gbit/s$ or above a very high accuracy of the fit to the measured group delay due to the low tolerance to dispersion.

2.6 Summary

In this chapter the effects of chromatic dispersion and higher order dispersion have been discussed in order to determine their influence on $160Gbit/s$ systems. The peculiar pulse shapes due to the third order dispersion was explained physically. The effect of fourth order dispersion was also explained. It was established that even though the third order dispersion length was much longer than the dispersion length it still was comparable to the transmission lengths used in optical communications systems. Thus in dispersion compensated systems the accumulated effects of third order dispersion must be compensated, prompting the necessity of slope compensation fibres. However the tolerance of the third order dispersion was argued to be much less stringent than the tolerance for the chromatic dispersion which was estimated to be around $\pm 2ps/nm$ for systems with a pulse width of $1.56ps$, for longer pulses the tolerance could be relaxed somewhat. For WDM purposes the requirement of the slope compensation was argued to be tighter than the requirements for compensation of the third order dispersion, due to the broader bandwidth needed for WDM system. The bandwidth of a $160Gbit/s$ channel is roughly $5nm$ compared to $50nm$–$100nm$ for WDM based systems. The fourth order dispersion was negligible at $160Gbit/s$ however expected to be important at even higher transmission rates. Due to the low residual dispersion tolerance of $160Gbit/s$ 100% slope compensation over a very broad wavelength range is necessary for WDM experiments at a rate of $160Gbit/s$.

Dispersion compensation using fibres, was discussed briefly and a PMD figure of merit was introduced, in order provide an easy way of estimating the

differential group delay of a dispersion compensating module from the desired total dispersion. The PMD FOM is a good parameter for evaluating the PMD of a DCF. The design of a slope compensation module was briefly discussed and it was seen that the dispersion of the fibre should be designed so that the inflexion point of the dispersion curve should be in the middle of the dispersion range used. Furthermore the RDS curve of the DCF should intersect the RDS curve of the transmission fibre twice and preferably the inflexion point of the dispersion curve should be in between the points of intersection. The broadest slope compensated range is achieved when the length of dispersion compensating fibre is matched at the middle wavelength with respect to the intersection wavelengths. The result for a slope compensating module for TW-RS based on the developed fibre called EHS was shown.

Due to the importance of the RDS for transmission systems at $160Gbit/s$ and WDM systems the measurement of the dispersion was investigated. Traditionally a fourth order polynomial or a 5-term Sellmeier has been used to measure the slope. It was shown that there were some great variations on the slope although no variations were seen on the fitted group delay curves by the naked eye. Furthermore a better precision was investigated. It was shown that re-scaling the abscissa to the range -1 to 1 before fitting improved the precision significantly. Furthermore it was shown that the fourth order polynomial and 5-term Sellmeier were inadequate as fitting functions to the measured dispersion for an EHS fibre. A polynomial of sixth degree proved adequate, and showed good agreement when compared with a measured curve for a span.

3. FIBRE NON-LINEARITY

The effect of Raman amplification on the fibre non-linear response is investigated. The experimental data presented are accompanied by a theoretical discussion. The results suggest that Raman amplification is a promising technique in realizing devises for optical telecommunication based on fibre non-linearity, in terms of controlling the fibre non-linear response. A non-linear enhancement factor of 3.8 was obtained experimentally using 382mW of counter directional pump with a 12.6THz frequency separation between pump and signal.

The non-linear properties of optical fibres used in telecommunication systems plays a dualistic role. While some systems are limited by non-linear pulse broadening, others take advantage of the pulse shaping properties of fibre non-linearity. Fibre non-linearity can be utilized for manipulation of the optical field carrying information, in devices such as wavelength converters, multiplexers and all optical regenerators.

Most non-linear effects in an optical fibre, e.g. self phase modulation, SPM, cross phase modulation, XPM, and four wave mixing, FWM, can be ascribed to the optical Kerr effect, which in a phenomenological approach can be accounted for by the real part of the time dependent third order non-linear susceptibility [24], $\chi^{(3)}$. The optical Kerr effect is often described through the non-linear refractive index, n_2. Owing to n_2 the fibre refractive index, $\overline{n}$, depends on the intensity of the propagating field through n_2 by the relation shown in equation 3.1. The non-linear refractive index is proportional to an average of the effect of $\chi^{(3)}$ over all possible light polarization states in the optical fibre.

$$(3.1) \quad \overline{n} = n_l + \frac{n_2}{A_{eff}} P$$

where P is the power of the propagating field and the effective area of the fibre is A_{eff}. n_l is the effective linear refractive index taking both wave guide effects and the material refractive index into account. Whereas generic SPM and XPM only change the phase of a given field, the generic FWM process changes both the amplitude and the phase of a given field depending on how well the phase of

the fields involved in the process is matched. These non-linear effects are mainly due to the fast electronic response of the wave-guide material to the optical field, however a significant contribution from the heavier nuclei is present [25].

The imaginary part of the third order susceptibility models the Raman effect. The Raman effect, which is due to the atomic response to the propagating optical field, only changes the amplitude of the optical field and leaves the phase invariant [39]. In fact the Raman effect is the interaction of two optical fields, with a large frequency separation, through an optical phonon[1]. In fused silica fibres the frequency separation is around 13THz. It is determined by the resonance of the molecular vibrations of the material at frequencies of tens of THz. The optical field with the larger frequency acts as an energy source for the lower frequency field, which is amplified. Thus stimulated Raman scattering allows the use of fibres as the amplifying media.

Brillouin scattering is another interaction with an optical field and acoustic phonons. Unlike the before mentioned non-linear effects, Brillouin scattering cannot be attributed to the third order susceptibility. The physical origin of Brillouin scattering is found in an effect called electrostriction, in which the optical field changes the local material density of the material, creating a material density wave. This density wave acts as a Bragg grating which reflects a fraction of the propagating optical field. The reflected field is shifted in frequency due to the Doppler effect. However below a certain threshold power this effect is insignificant.

Raman amplification is becoming widely spread due to the emergence of very high power semiconductor lasers, and is used both as distributed amplification in transmission fibres and as lumped amplifiers in dispersion compensating modules based on dispersion compensating fibre technology. Thus it is important to assess the limitation posed on at transmission system due to enhanced fibre non-linear response caused by Raman amplification.

3.1 Enhancement of non-linear effects using Raman amplification

In this section the theory of Raman enhanced non-linearity is discussed. Starting with a very simple approach an analytical expression of the Raman enhanced non-linearity is derived for the special case where only one signal is propagating in the fibre i.e. only SPM is taken into account. Initially SPM is briefly discussed

---

[1] More precisely the Raman effect is due to the interaction of the optical fields and the nuclei or molecules. Due to the amorphous structure of the fibres use of the term phonon is not applicable.

using a generalized Schrödinger equation in which a general expression for the power evolution along the length of fibre is used. Secondly Raman amplification in the case of continuous wave (cw) and no pump depletion is treated. XPM between pump and signal is being neglected.

3.1.1   The generalized NLS

The governing equation for pulse propagation in an optical fibre is the non-linear Schrödinger equation, which is derived in appendix A. The complex field amplitude, $A(z,t)$, of an optical pulse can be described as follows

(3.2) $A(z,t) = \sqrt{P(z)}u(z,t)$

Where $u(z,t)$ describes the normalised complex envelope of the field, and $|u(z,t)|^2$ is the temporal distribution of the optical field evaluated at a given length of the fibre.

(3.3) $P(z) = P_0 \exp(f(z))$

$f(z)$ is a real non-zero function describing the evolution of the peak power along the length of the fibre. In most cases $f(z) = -\alpha z$ in which case $P(z)$ just describes the effect of fibre attenuation. The evolution of the complex field amplitude, which is governed by the non-linear Schrödinger equation [24], is shown in equation 3.4.

(3.4) $i\dfrac{\partial A}{\partial z} = \left[i\dfrac{\partial}{\partial z}\dfrac{f(z)}{2} + \dfrac{1}{2}\beta_2\dfrac{\partial^2}{\partial t^2} - \gamma|A|^2 \right] A$

where β_2 is the second order dispersion, and $\gamma = 2\frac{\omega_0}{c}\frac{n_2}{A_{eff}}$, where ω_0 is the central angular frequency of the optical field and c is the velocity of light in free space. Substituting equation 3.2 into equation 3.4 we obtain the governing equation for the normalized complex envelope distribution.

(3.5) $i\dfrac{\partial u}{\partial z} = \left[\dfrac{1}{2}\beta_2\dfrac{\partial^2}{\partial t^2} - \gamma P(z)|u|^2 \right] u$

The first term on the right hand side of equation 3.4 modeling the power evolution in the fibre vanishes and only the two latter terms remain, however the power evolution is included in P. Equations equation 3.2 and equation 3.5 will

be the starting point of the subsequent discussion of Raman enhanced non-linearity. For simplicity the effects of dispersion will be neglected in the following. Omitting the effects of chromatic dispersion equation 3.5 is readily integrated yielding.

(3.6) $u(z,t) = u(0,t)\exp(i\gamma P_0|u|^2 L_{eff})$

where

(3.7) $L_{eff} = \int_0^z dz' \exp(f(z'))$

is the effective length. Using $f(z) = -\alpha z$ the effective length is easily integrated to give the well-known effective length $L_{eff} = \frac{1-\exp(-\alpha L)}{\alpha}$, which later on will be taken as a reference to the non-linear response of a fibre. In equation 3.6 it is seen that the effect of SPM is to change the phase of the propagating pulse, whereas the temporal distribution of the pulse is left unchanged. The non-linear phase shift of SPM, φ_{SPM}, is given by

(3.8) $\varphi_{SPM} = \gamma P_0|u|^2 L_{eff}$

The magnitude of φ_{SPM} for a given fibre can be controlled by choosing the input power, P_0 , and L_{eff}, since γ is a fixed parameter for the particular fibre. L_{eff} corresponds to the length of a loss less fibre, in which the power is held constant along the length of the fibre, that gives the same φ_{SPM} as the physical fibre. Thus L_{eff} takes the evolution of the power of the propagating optical field into account through the integral in equation 3.7. In the usual case without Raman gain it is worthy to notice that the effective length is limited by the attenuation i.e. $\lim_{L\to\infty}(L_{eff}) = \alpha^{-1}$. Thus regardless of how long a fibre length is chosen the non-linear effect cannot exceed the effect of a loss less fibre with a length of α^{-1} . This is true, only in the case where the power of the optical field is governed by the fibre attenuation.

In equation 3.8 it is indicated that chromatic dispersion tends to lower the effect of SPM since the pulse is broadened in time by the group velocity dispersion, and thus the magnitude of $|u(z,t)|^2$ is lowered. No further investigation of the effect of chromatic dispersion on fibre non-linearity will be pursued at this point.

3.1.2   Raman enhanced non-linearity

In this section Raman amplification and the effect it imposes on the fibre non-linearity is discussed. In the case of continuous wave the interaction between

the intensities of the pump wave, I_p, and the Stokes wave, I_s, can be described by a set of coupled differential equations 3.9 and 3.10 [24].

(3.9) $\quad \dfrac{dI_s}{dz} = g_R I_p I_s - \alpha_s I_s$

(3.10) $\quad \dfrac{dI_p}{dz} = -g_R \dfrac{\omega_p}{\omega_s} I_s I_p - \alpha_p I_p$

It is seen that the pump is attenuated both due to the fibre attenuation and due to the Raman effect, which transfers energy from the pump to the Stokes wave. Providing the pump intensity is adequate the Stokes wave is amplified. Assuming that the pump wave is not depleted, the first term on the right hand side of equation 3.10 can be neglected, and the coupled equations are readily solved, by integrating equation 3.11, where P_p^0 denotes the initial pump power injected at any length.

(3.11) $\quad \dfrac{dI_s}{dz} = \left[\dfrac{g_R}{A_{eff}} P_p^0 \exp(-\alpha_p z) - \alpha_s \right] I_s$

yielding in the case of co-propagating pump—forward pumping scheme.

(3.12) $\quad P_s(z) = P_s(0) \exp\left(\dfrac{g_R}{A_{eff}} P_p(0) \dfrac{1 - \exp(-\alpha_p z)}{\alpha_p} - \alpha_s z \right)$

since $I = \frac{P}{A_{eff}}$. Equation 3.12 thus evaluates the Stokes power evolution along the length of the fibre. It is straightforward to verify by a coordinate transformation, that in the backwards-pumping scheme, where the pump wave is injected counter directionally at the fibre length, L, the power evolution is given by equation 3.13.

(3.13) $\quad P_s(z) = P_s(0) \exp\left[\dfrac{g_R}{A_{eff}} P_p(L) \exp(\alpha_p(z - L)) z_{eff} - \alpha_s z \right]$

where $z_{eff} = \frac{1 - \exp(-\alpha_p z)}{\alpha_p}$. In the case where bi-directional propagating pump waves are used to amplify the Stokes wave equation 3.12 and equation 3.13 can readily be combined to yield

(3.14) $\quad P_s(z) = P_s(0) \exp\left(\dfrac{g_R}{A_{eff}} z_{eff} \left[P_p^f(0) + P_p^b(L) \exp(\alpha_p(z - L)) \right] - \alpha_s z \right)$

where the superscripts denotes whether the pump wave is used in the forward or the backward scheme. Equations 3.12–3.14 all have the form of equation 3.3

and thus can easily be inserted into equation 3.5 to assess the effect of Raman amplification on the fibre non-linear response. In the case of negligible chromatic dispersion it is seen that the effect of Raman amplification is to enhance the effective length given by equation 3.7 and thereby enhancing the non-linear response of the fibre. It is interesting to notice that the enhancement of L_{eff} does not depend on the input power of the signal, but on the input power of the pump. Leaving the possibility to tune the non-linearity of the fibre by varying the pump power into the fibre.

From equation 3.8 it can easily be seen that the non-linear enhancement factor, R_e, due to Raman amplification is given by the ratio of the effective length with Raman amplification to the effective length in the case without pump. R_e is given by equation 3.15 in the backward pumping case. Which is evaluated numerically.

$$(3.15)\quad R_e = \frac{\alpha_s}{1 - \exp(\alpha_s L)} \int_0^L dz \exp\left[\frac{g_R}{A_{eff}} P_p^b(L) \exp(\alpha_p(z - L)) z_{eff} - \alpha_s z \right]$$

3.2   Experimental set-up

In this section the experimental set-up for measuring the Raman enhanced non-linearity in the backward pumping scheme is described. The set-up employs a well-known technique of measuring the non-linear phase shift of a continuous wave beat signal. The experimental set-up for measuring the enhancement of the fibre non-linearity due to backward Raman amplification is shown in Fig. 3.1.

The non-linear phase shift is measured by injecting a dual wavelength cw beat signal into the fibre under test (FUT). The non-linear phase shift is thus determined by the ratio between the intensity of the fundamental wavelength, I_0, and the intensity of the first order side band, I_1, through the relation given in equation 3.16 [37]

$$(3.16)\quad \frac{I_0}{I_1} = \frac{J_0^2(\varphi_{SPM}/2) + J_1^2(\varphi_{SPM}/2)}{J_1^2(\varphi_{SPM}/2) + J_2^2(\varphi_{SPM}/2)}$$

where the non-linear phase shift due to self phase modulation is given by

$$(3.17)\quad \varphi_{SPM} = 2\frac{\omega_0}{c}\frac{n_2}{A_{eff}} L_{eff} \overline{P}$$

The beat signal is realised by the tuneable lasers. The polarisation controllers and the polarizer are used to assure that the two waves have the same

polarisation state after being coupled into one fibre by the 3dB coupler. The EDFA is used to amplify the signal to a high power level. The DA-100 variable attenuator is utilised to control the power inserted into the fibre under test (FUT). The 1% tap is used to monitor the input power into the fibre. The first WDM is used to decouple the pump wave, allowing the monitoring of the pump output power. The second WDM is used to couple the pump wave into the FUT. Two isolators have been inserted to protect the periphery equipment from the pump wave. The FUT is pumped by the backward pumping scheme. The spectrum of the light passing through the FUT is obtained by the optical spectrum analyser (OSA), which is protected from possible excessive power levels inherent in the method by the HP attenuator. The monitored powers are measured using an optical power meter.
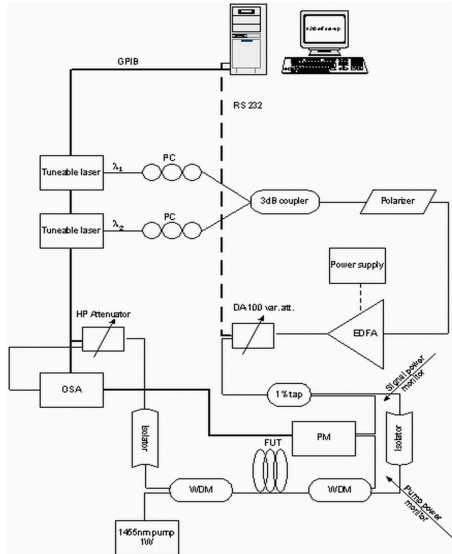
Fig. 3.1: The experimental set-up is shown. The thin full lines represent the optical path, starting from the tuneable lasers. The thick full lines represent the GPIB bus. The thick dashed line represents an RS 232 connection. And the dashed line represents an electrical power cord.

The FUT is spliced into the set-up to ensure that the power into the fibre does not depend on possible mechanical instabilities. The measurements are carried out, by measuring the ratio between the fundamental and the first order side

bands using the OSA, and the corresponding signal power at different pumping
levels. Further to correctly asses the pump power injected in the FUT the
output pump power is measured while signal power is turned off using the Da-
100 attenuator in order to avoid pump depletion effects in determining the pump
power. Two cut back measurements are made at the end of the measurement
series to eliminate the unknown splice losses.

3.3   Results
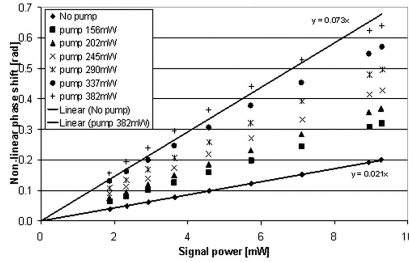
Fig. 3.2: Shows the non-linear phase shift as a function of signal power. The
case with no pump is used as a reference to evaluate the non-linear
coefficient. Furthermore the fit to the data is used as a reference to
calculate the non-linear enhancement factor.

In this section the results of a measurement series on a 2.1km highly non-
linear fibre (HNLF) is presented along with some theoretical predictions based
on parameters from the same fibre. The HNLF was chosen due to a very low
dispersion, which justifies the neglect of the dispersion in equation 3.6. The
experimental set-up shown in Fig. 3.1 was used to measure the non-linear
phase shift induced by the FUT subject to a high signal power level.

The wavelength of the pump used is 1455nm, and the signal wavelength has
been chosen to be 1550nm. The wavelength separation of the two signals was
0.2nm. The attenuation of the fibre was 1.01dB/km and 0.779dB/km for the
pump and signal wavelength respectively. In Fig. 3.2 the non-linear phase shift
as a function of signal input power is shown for various pump powers. It is clearly
seen that the Raman amplification does enhance the non-linearity of the fibre.
As expected from equation 3.8 the non-linear phase shift at a given pump power
is proportional to the signal input power. However the topmost line does not fit
well to a straight line; at high signal powers the non-linear phase shift tends to

saturate. This inconsistency with theory can be attributed to stimulated Brillouin scattering of the signal, however in this case this behaviour could also be accounted for by pump depletion. The curve obtained with an idle pump is used
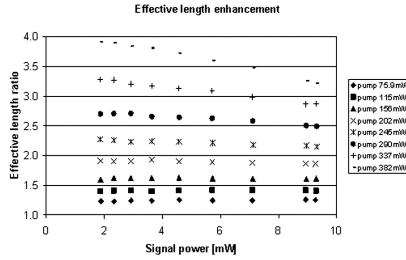
Fig. 3.3: The enhancement of the effective length is shown. As anticipated the enhancement factor does not depend on signal power at small pump powers. At high pump powers the effect of pump depletion and stimulated Brillouin scattering is seen, as the enhancement factor decreases with signal power.

as a reference non-linear phase shift or effective length. By performing a least squares fit to the data an expression for line is obtained. Thus the non-linear coefficient, $\frac{n_2}{A_{Eff}}$, can be determined and the non-linear enhancement factor due to Raman amplification can be found simply by evaluating the ratio of the non-linear phase shift without Raman pump to the non-linear phase shift obtained with the Raman pump active. $\frac{n_2}{A_{Eff}}$ was determined to be $1.4910^{-9}W^{-1}$. Fig. 3.3 shows the non-linear enhancement factor at different pump powers. It is seen that a maximum enhancement factor of 3.8 is obtained with 382mW pump power. At low pump powers the enhancement factor is independent of the signal power as anticipated from the theoretical discussion. However stimulated Brillouin scattering and pump depletion lowers the non-linear enhancement factor for increasing signal powers as seen on the uppermost curves in Fig. 3.3. Thus it is necessary to suppress the stimulated Brillouin scattering i.e. increase the threshold power. Further this independence of the input power could be used to tune the non-linear response of a device. The Raman gain of the fibre used has been measured in order to compare the measured non-linear enhancement to the theoretical prediction equation 3.15. The Raman gain efficiency, $\frac{g_R}{A_{eff}}$, is shown in Fig. 3.4. The abscissa represents the frequency shift of the Raman scattered optical field relative to the pump frequency. The frequency separation of the experiment is 12.6THz yielding a Raman gain efficiency of $4.4(Wkm)^{-1}$.
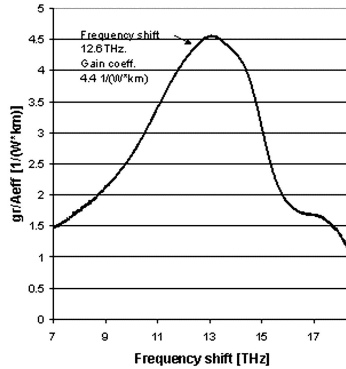
Fig. 3.4: The Raman gain efficiency as a function of frequency shift relative to the pump. The gain efficiency at 12.6THz is used in the theoretical calculations.
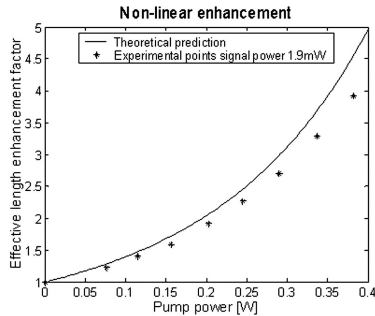
Fig. 3.5: Comparison between experimental results and calculations using equation 3.15. The experimental points are taken for the lowest input signal power of 1.9W.

The fibre data has been used to calculate the non-linear enhancement factor, R_e, in the case of a counter directional pump scheme. Further the experimental data presented in Fig. 3.3, which is corresponding to the lowest signal power is compared to the calculation. Since these data points are least affected by SBS and pump depletion. This comparison is shown in Fig. 3.5.

It is seen in Fig. 3.5 that there is a fairly good agreement between experiment
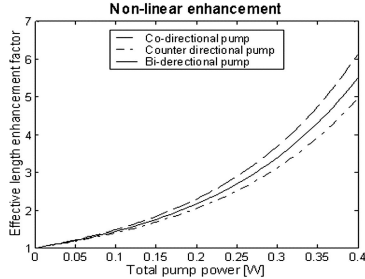
Fig. 3.6: Theoretical calculation of using co-, counter, and bi-directional pumping schemes. The total pump power in all three cases is the same. Symmetrical pump powers are used in the bi-directional case.

and theory. The discrepancy between experiment and theory could be attributed to pump depletion and stimulated Brillouin scattering of the signal. The pump is depleted mostly by SBS of the pump, however some depletion due to energy transfer to the stokes wave can not be ruled out.

Fig. 3.6 shows some theoretical calculations of R_e for co-, counter-, and bi-directional pumping schemes. The total power is the same in each case. In the case of bi-directional pump the pump powers are symmetrical, i.e. $P^f(0) = P^b(L) = \frac{1}{2}P_{tot}$. It is seen that the co-propagating scheme yields the largest non-linear enhancement, whereas the counter directional pump scheme results in the lowest non-linear enhancement for the same total power. The non-linear enhancement for the bi-directional pumping scheme lies somewhere between the other schemes depending on the ratio of the pump powers used. It is clearly, that not only does Raman amplification enhance the fibre non-linear response, but moreover this enhancement could be tuned by varying the pump power, or by proper choice of the pumping ratio in the bi-directional case.

3.4 Summary

In order to asses the effect of Raman amplification on the non-linear response of an optical fibre some simple theoretical considerations along with experimental verification have been performed.

Although XPM between pump and signal was neglected in this case the experimental data point fits very well with theory. Nevertheless in future experiments countermeasures against SBS must be employed, and the theory must at least be expanded to entail the effects of pump depletion, which would introduce

a slight dependency of the signal input power. However in most practical cases chromatic dispersion of the fibre cannot be neglected and must be incorporated in the theory.

Assuming that the only interaction between the pump and the signal is stimulated Raman scattering, no pump depletion, cw pump, negligible effect of chromatic dispersion, and a slowly varying envelope it was shown that the non-linear enhancement factor, R_e, due to Raman amplification was independent on the signal input power. Furthermore tuning of R_e can easily be done by varying the power of the pump and by proper choice of pumping scheme. The non-linear enhancement is due to power evolution of the signal when Raman amplification is applied to the fibre.

An experiment using a 2.1km long HNLF, with $\frac{n_2}{A_{eff}} = 1.49 \, 10^{-9} W^{-1}$ was performed to test the theory. The pump and signal wavelengths used were 1455nm and 1550nm respectively corresponding to a frequency shift of 12.6THz. Using a 382mW pump an enhancement factor of 3.8 was obtained. The Raman gain efficiency was measured for the test fibre resulting in $\frac{g_R}{A_{eff}} = 4.4 (Wkm)^{-1}$. A small discrepancy between theory and experiment was observed. This could be ascribed to the effects of pump depletion and SBS.

Raman amplification shows a great potential to enhance the fibre non-linearity and to realize devices for optical communication systems based on non-linear effects in optical fibres with dynamic control of the fibre non-linear response.

4. SYSTEM EXPERIMENTS

In this chapter system experiment at $40Gbit/s$ and $160Gbit/s$ are presented. Raman amplification is shown to increase transmission length considerably due to improved signal to noise ratio [40].

Experiments at $160Gbit/s$ have allready been reported in literature [2, 3, 41], however a comparison af four different fibre types are presented for the first time, indicating that high dispersion low non-linearity fibres are performing best, due to the limitations of intra channel non-linear effects [42].

4.1 40Gbit/s single channel transmission

In this section the system experiments at COM is presented. The work was done in collaboration with Christophe Peucheret and Torge Torkle in particular. All the transmission experiments performed at COM were single channel $40Gbit/s$ OTDM experiments. Both the experiments presented where done using the re-circulating set-up available at COM. The effect of Raman amplification was investigated in both experiments. The experiments were carried out on TW-RS and EHS fibres. The $40Gbit/s$ signal was obtained by optical time division multiplexing a signal stream at $10Gbit/s$. The clock was co-propagated and separated from the data signal at the reciever end.

4.1.1 Experiments January 2001

In this first experiment in a series of two we compared the performance of a single $40Gbit/s$ channel with and without Raman amplification. One $80km$ TW-RS span compensated by an EHS dispersion compensating module was used in the re-circulating loop [43]. The co-workers in this experiemnt are Torge Tokler, Christophe Peucheret and Marco Girimondo.
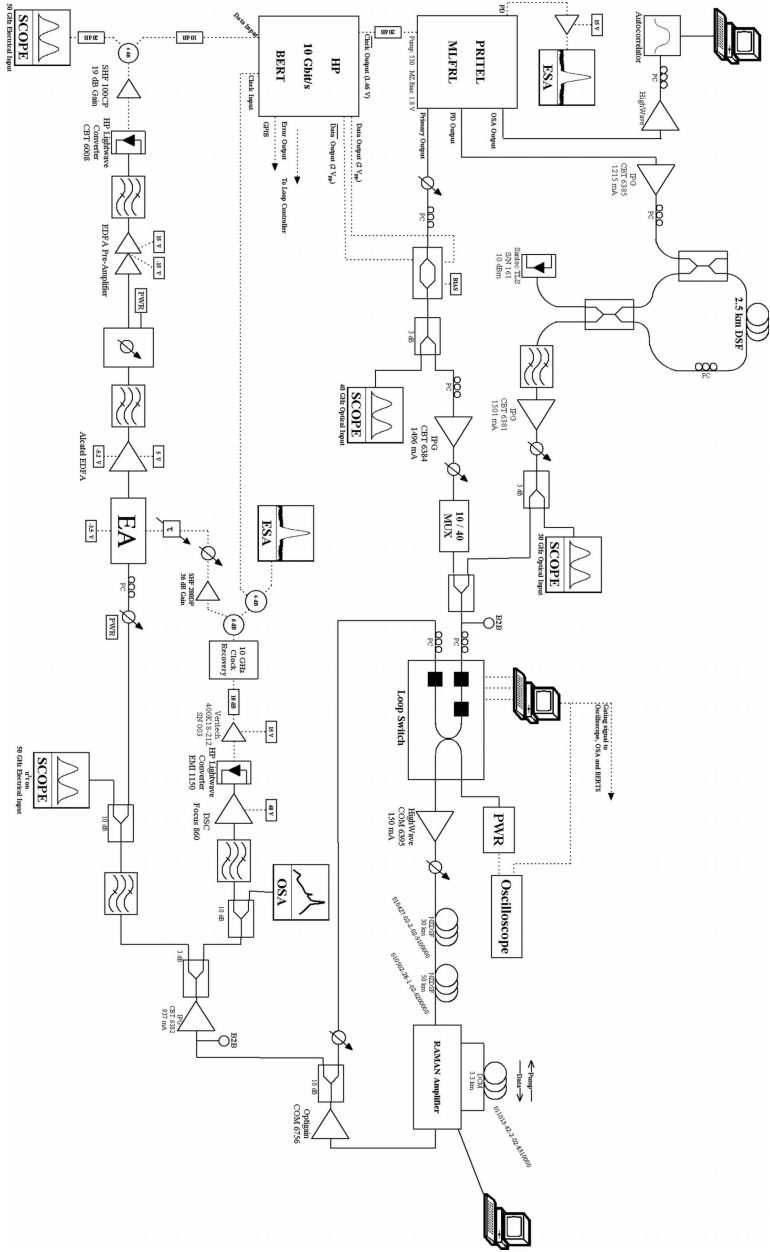
Fig. 4.1: The set-up of the single channel 40Gbit/s experiment at COM, [Torge Tokle].

Set-up

In this section the experimental set-up used in both experiments is presented in figure 4.1. Torge Tokle has produced the figure and kindly allowed its use in this thesis.

Transmitter. The transmitter which is depicted on the left upper part of figure 4.1 consist of two parts. The first part is used to generate the $40Gbit/s$ signal. The $10GHz$ data stream at $1559nm$ was taken from a modelocked fibre ring laser from Pritel. Provided a $10GHz$ pulse stream with a FWHM pulse width of $\sim 3.3ps$. The pulse stream was modulated using a LiNbO$_3$ Mach-Zehnder modulator, which was driven by the data stream and inverted data stream from the bit pattern generator. The modulated signal is split by a $3dB$ splitter, in order to monitor the modulated signal on an optical oscillation scope. The signal is passed through an optical amplifier and then injected into the 10:40 mulitiplexer. The $40Gbit/s$ signal is then combined with the 10GHz clock in a $3dB$ coupler. The combined $40Gbit/s$ signal and $10GHz$ clock from the coupler was used as the back to back point of the transmitter.

The clock was taken from the Pritel laser as well. The clock was shifted to a wavelength of $1552nm$ by a non-linear optical loop mirror, NOLM [44], with 2.5km of dispersion shifted fibre inserted. A continuous wave (cw) laser was used to provide the wavelength of the transmitted clock. The wavelength converted clock was then passed through a bandpass filter to ensure that only the converted clock was allowed to pass. The converted clock was then amplified by an optical amplifier before it was combined with the multiplexed data signal. The combined data and clock was transmitted into the re-circulating loop.

Receiver. The data from the re-circulation loop were amplified before it was split in order to extract the clock from the signal. In the clock recovery arm of the receiver the signal was filtered out by a bandpass filter set at the clock wavelength. After the amplifier the optical clock signal is converted into an electrical signal using a light wave converter. The electrical signal is amplified and the clock extracted by a $10GHz$ clock recovery. The recovered clock is split and used to trig the bit error rate test set and drive the electroabsorption (EA) modulator used to de-multiplex the $40Gbit/s$ data to a $10Gbit/s$ signal.

In the other arm the filtered signal is transmitted through a polarization controller into the EA-modulator which serves the purpose of demulti-

plexing the $40Gbit/s$ signal back to a $10Gbit/s$. The EA is driven by the recovered clock, however a time delay is inserted between the clock recovery circuit and the EA. The time delay is mainly used to synchronize the clock and data signals at the EA; for a straight line experiment the delay line would also serve the possibility to test the performance of all the OTDM tributaries of the $40Gbit/s$ signal, however when the recirculating loop setup is used each tributary is in fact an average of all the channels due to the fact that the loop switches are not synchronized to the data signal. After the EA the $10Gbit/s$ signal is filtered and passed through a variable attenuator, which determines the input optical power into the detection circuit of the receiver i.e. the sensitivity of the receiver is defined as the optical power at this point which gives a BER of 10^{-9}. The detection circuit consists of an optical pre-amplifier, a bandpass filter, a wavelength converter, and an electrical pre-amplifer which is placed in front of the $10Gbit/s$ test set.

Span. A single $80km$ TW-RS span with approximately $3km$ of EHS DCM is used in the loop, by letting the data circulate in the loop several times multiple spans can be simulated. An optical amplifier is used to compensate the insertion losses of the loop switches and a variable attenuator is used to control the input power into the fibre span. The DCM is placed after the transmission span. The DCF is Raman pumped in the counter directional scheme. The Raman pump consists of three pump lasers at different wavelengths in order to have a flat gain profile over a wide wavelength range, which is most interesting for WDM applications. The Raman pump was build by Carsten G. Jørgensen at OFS Fitel Denamrk. The optical powers of the pump could either be coupled out after the DCM or it could be propagated into the transmission fibres as well. An optical amplifier is placed behind the fibre span. It should be noted that the optical field is split for monitoring purposes at several occasions not described in the earlier description of the set-up.

Results

In this section the result of the experiment are discussed. Firstly we investigated the effect of Raman amplification in term of optical signal to noise ratio by measuring the spectra at the output of the Raman pumped DCM with the pumps on and off. Through out the experiments all three pumps were set at $230mW$ each. The spectra from the output of the DCM were measured with

and without the Raman pumps. This Raman on/off gain measurement were performed at three different settings. Firstly we measured the on/off Raman gain in the cases where only the DCM and the transmission fibre were pumped respectively i.e. the performance of discrete and distributed Raman amplification were tested. Furthermore we investigated a hybrid amplification scheme where the pump was propagated through both the DCM and transmission fibre. The power into the fibres were optimized and then kept constant.

(a) DCM

(b) NZDSF

(c) DCM+NZDSF
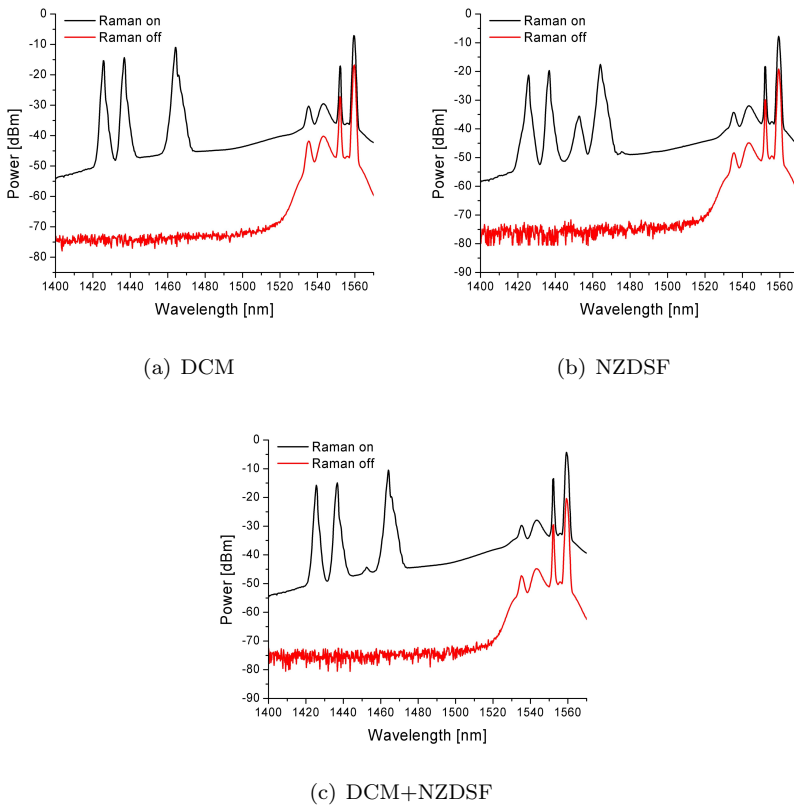
Fig. 4.2: Raman spectra

Figure 4.2 shows the measured spectra, the two smaller peaks around the signal wavelength are from due to the erbium amplifier used. The black lines all

represent the case where the Raman pumps were on and the red curves depict
the cases without pumps. The optical power arising from the back scattered
pumps is seen on all the figures. In figure 4.2(b), where the spectra for the
non-zero dispersion shifted fibres are shown it is seen that there is an additional
component building between the pump fields. This is due to four wave mixing
of the individual pumps. In spectra of the DCM in figure 4.2(a) this FWM
component does not show at all. The reason for the absence of FWM in the
DCM is that there is a significant amount of dispersion at the pump wavelengths
in the dispersion compensating fibre, whereas the zero dispersion wavelength of
the transmission fibre used is around $1450nm$, which is among the pump wave-
lengths. However in the total pumping scheme, where both the DCM and the
transmission fibre are pumped shown in figure 4.2 the FWM product is reduced
drastically. The pump-pump interaction occurring in the transmission fibre may
cause some penalties to system performance and the distributed Raman scheme
is therefore not used in the following experiments. The Raman on/off gains
were measured by measuring the peak power of the signal at $1559nm$ with the
pump turned on and off. The on/off gain obtained when pumping the DCM is
$9.7dB$ whereas the total pumping scheme yielded an on/off gain of $16.2dB$.

(a) 6 RT   (b) 10 RT
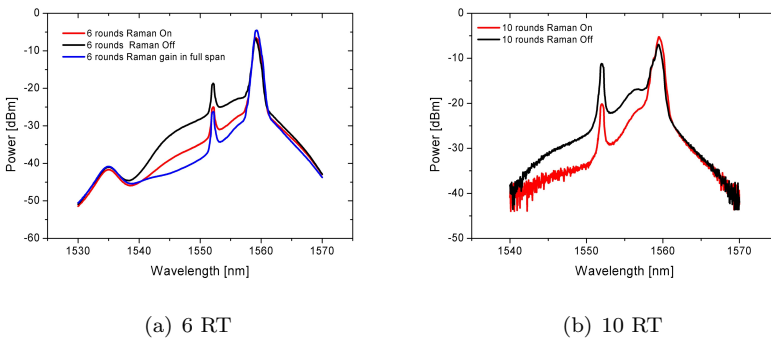
Fig. 4.3: The optical spectra after six roundtrips and ten round trips shown
            in (a) and (b) respectively.

We measured the spectra of the optical field transmitted into the receiver.
The OSNR was estimated by measuring the peak power used and the power
value at a wavelength $2.5nm$ less than the wavelength of the peak. This proce-
dure was done for the cases where the signal had circulated six and ten times in

the loop respectively. In figure 4.3 the measured spectra is measured. In figure 4.3(a) the spectra for six roundtrips are shown, The black curve corresponds to the case where the Raman pumps are off, the red curve is obtained by including Raman amplification in the DCM, and the blue is for the total pumping case. An improvement of $4.4dB$ was obtained when only the DCM was pumped, whereas in the total pumping case an increase of $8.6dB$ in the OSNR compared to the non pumped case was obtained. Despite the better performance in terms of OSNR improvement the total pumping capacity was not used in the transmission experiments due to higher influence of fibre non-linearity. Thus only the pumping of the DCM was used in the transmission experiments. For ten roundtrips the addition of the Raman pump improves the OSNR by $6.1dB$, which is seen in figure 4.3(b).

(a) Pulse   (b) Dispersion
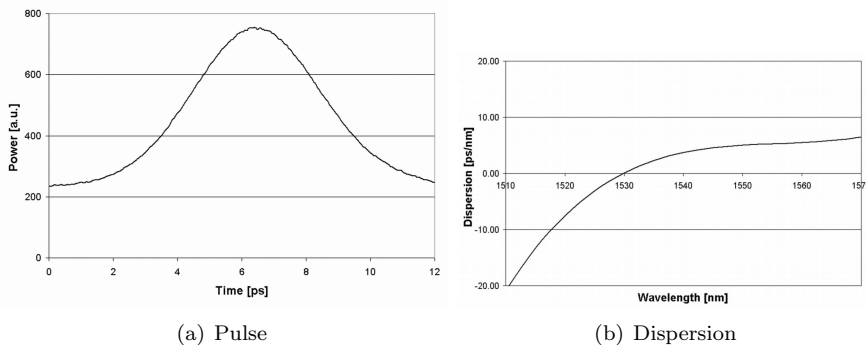
Fig. 4.4: The pulses from the Pritel laser is shown in (a). In (b) the residual dispersion of the span is shown.

We measured the pulse width of the mode locked laser on an autocorrelator. The autocorrelation trace shown in figure 4.4(a). The measured FWHM pulse width is $4.64ps$ on the autocorrelator, corresponding to a FWHM pulse width of $3.3ps$ assuming a Gaussian pulse. In order for the pulse to broaden so that the FWHM is equal to the bit slot, which is $25ps$ for a transmission rate of $40Gbit/s$, the pulse must propagate through a length of fibre which corresponds to approximately eight dispersion lengths or a total dispersion of $D \approx 25ps/nm$, since the dispersion length in this case is approximately $0.61km$. From figure 4.4(b), where the measured span residual dispersion is shown, the residual dispersion at $1559nm$ of $5ps/nm$ is obtained. Thus it is expected that the transmission would be limited by dispersion after five or six roundtrips in the loop.

(a) 4 RT   (b) 5 RT
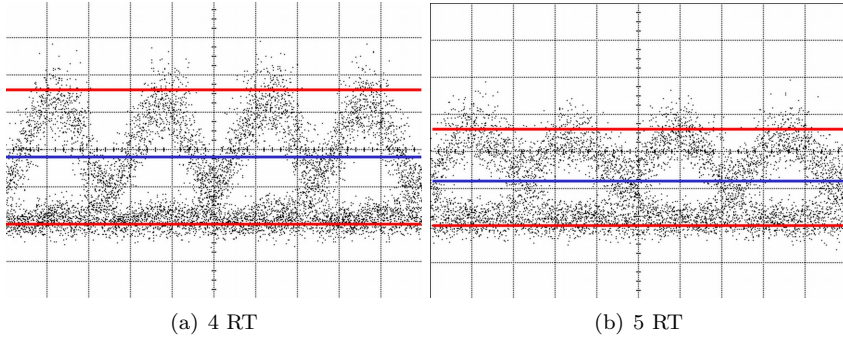
Fig. 4.5: The optical eyes after four roundtrips and five round trips shown in
(a) and (b) respectively.

In figure 4.5 the effect of dispersion is seen in the eye diagrams taken at
the receiver. Figure 4.5(a) shows the eye after four roundtrips and figure 4.5(b)
shows the eye after five roundtrips. The eyes were taken after four and five
roundtrips in the loop. Raman amplification of the DCM was applied. The
blue lines represents the half maximum power, which is deduced from the red
lines estimating the 'one' and 'zero' levels. It is seen that the half maximum
power after four roundtrips lies above the point where adjacent pulses start to
overlap, whereas the overlap point is coinciding with the half maximum power
point in figure 4.5(b) as expected from the previous estimations.

In fact we measured the performance of the system while changing the num-
ber of spans and were not able to achieve an error free transmission after seven
roundtrips due to the impairment of the accumulated dispersion of $35ps/nm$.
Thus in addition we inserted additional $-30ps/nm$ of dispersion compensation
before the receiver after the re-circulating loop and repeated the measurements.
Figure 4.6(a) shows the measured bit error rate curves for the experiment with
added dispersion compensation. The power penalty, which is defined as the
difference in receiver sensitivity at a BER of 10^{-9} compared to the B2B case,
is found in both experiments and plotted in figure 4.6(b). The power penalty
curve is plotted against the transmitted distance, which is related to the num-
ber of roundtrips since the span length is $80km$. The red curve depicts the
results from the experiments with additional dispersion compensation, and the
black curve is taken without the additional dispersion compensation. We were
able to increase the transmission length by introducing the additional dispersion

compensation.

(a) BER
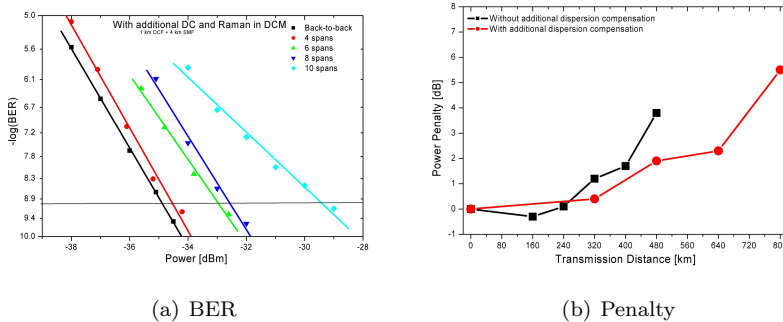
(b) Penalty

Fig. 4.6: (a) shows the BER curve for the experiment with additional dispersion compensation. In (b) the power penalty is shown.

The power penalty is not an absolute measure of the performance of the system since the effects of averaging due to the re-circulating loop is not taken into account when measuring the B2B curve. However it shows the trend of the performance.

In figure 4.7 the BER curves after ten roundtrips are shown. The black curve is the B2B performance. The red points are taken with the Raman pump on. The blue point are taken without Raman pump. Error free transmission was not achieved without Raman amplification as an error floor occurred as seen on figure 4.7. The eyes show that the noise limits the transmission.

4.1.2 Experiments May 2002

The experiments presented in this section is the second of the experiments series at COM. The Transmitter and receiver set-up was the same as the previous experiments described in section 4.1.1. The receiver senitivity was $-38dBm$. Two single channel transmission experiments were performed, one with transmission over $2 \times 80km$ TW-RS and EHS dispersion compensating fibre and one where transmission over one $160km$ span is investigated. Both experiment were done with Raman amplification. Two fibre spans were prepared very carefully in order to reduce effects of accumulated dispersion. The residual dispersion at the signal wavelength $1559nm$ was only $-1.1ps/nm$ giving very close to 100% dispersion compensation. Close to 100% slope compensation was also obtained
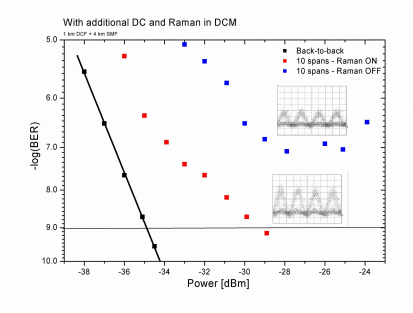
Fig. 4.7: The performance of the system with and without Raman amplification is compared after ten roundtrips.

as seen in figure 4.8. The black curve is the residual dispersion with the scale on the right hand side of the graph and the red curve is the signal and clock spectra. The pulse width of the pulses was measured to $2.8ps$ on the autocorrelator. The clock wavelength was $1552nm$ as in the previous experiments.
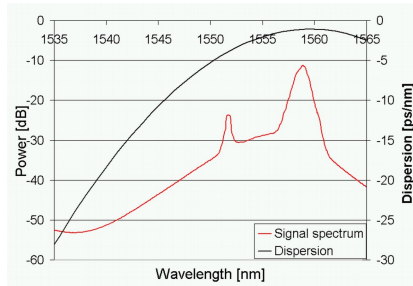
Fig. 4.8: The residual dispersion of both spans used in the experiments.

Results $2 \times 80km$ spans experiment

The span setup for the $2 \times 80km$ spans experiment is shown in figure 4.9. The Raman pump laser at $1455nm$ available for this experiment provided $30dBm$ of output optical power. The output from the laser was split by a $3dB$ coupler and coupled into the fibre spans via the DCM using a WDM coupler. The two spans were both pumped in the counter directional scheme. A quick investigation indicated that the optimum performance was obtained with 11.5dBm Raman pump

power per span, which corresponded to $7.7A$ of driving current to the Raman pump. An additional $90m$ of SMF was placed at the receiver in order to trim the dispersion. The main difference compared to the previous experiment was
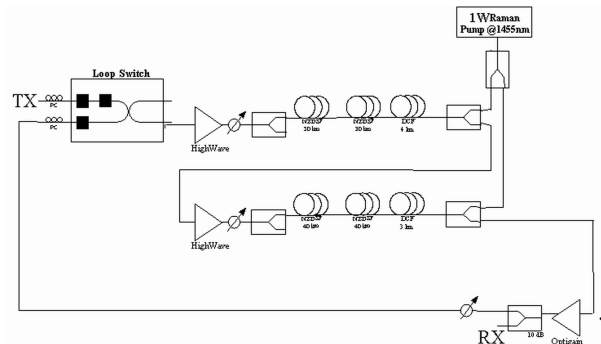
Fig. 4.9: The loop set-up in the $40Gbit/s$ transmission system experiments. [Torge Tokle]

the number of spans used in the loop, which were increased to two spans. This was done in order to limit accumulated detrimental effects, such as polarization mode dispersion, due to the repeated propagation in the spans. Thus a longer transmission length was expected compared to the previous. Furthermore we carefully matched the spans in order to compensate dispersion and slope completely. The Raman pump used only consisted of one pump wavelength contrary to three in the previous experiment, which in fact for single channel transmission was abundant, due to the limited bandwidth required compared to WDM systems. A WDM experiment with $32 \times 40Gbit/s$ on standard single mode fibre using hybrid Raman and EDFA amplifiction were in fact performed in collaboration with Alvaro Buxens, Tellabs Denmark, during the project. A discussion on the results obtained, however, is outside the scope of this thesis [45].

The power penalty versus transmission distance was measured in three cases. The first measurement was carried out without Raman amplification and additional dispersion trimming, which is shown as the blue curve in figure 4.10. The second measurement shown in the black curve were still without the use of Raman amplification, however with the additional dispersion trimming of $\sim 1.6ps/nm$. Finally Raman amplification was utilized along with the dispersion trimming. The maximum transmission distance was obtained in the measurement using Raman amplification and dispersion trimming. The maximum
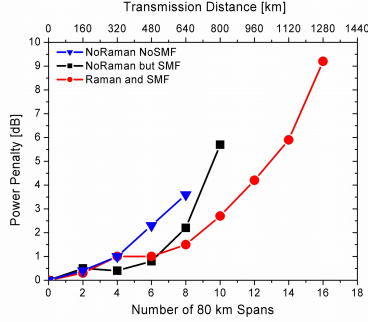
Fig. 4.10: The penalty vs. transmission length is shown.

transmitted distance was $1280km$. The Raman amplification gave $6.2dB$ and $8dB$ of signal on/off gain for the first and second span respectively. However without Raman the additional $\sim 1.6ps/nm$ dispersion at the receiver increased the transmission distance from $640km$ to $800km$.

The span losses were $22.8dB$ and $21.6dB$ for the first and second span respectively. The accumulated dispersion in the first measurement was $-4.4ps/nm$, whereas the accumulated dispersion with the additional SMF was $-3.8ps/nm$. Assuming a Gaussian pulse shape the dispersion tolerance can be estimated to $\pm14ps/nm$ which is much higher than $-4ps/nm$. Thus the system was not dispersion limited, and the fact that the added dispersion fibre improved the transmission in terms of transmission length indicates that the system is not limited by noise, however non-linear impairment is the most probable cause for the limitations seen. The signal input power which was optimized using an opti-

RB [nm]	Span 1	Span 2
0.5	3.5dBm	2.0dBm
1	5.9dBm	4.4dBm
2	7.7dBm	6.3dBm

Tab. 4.1: The optimum signal input power into the spans measured using an optical spectrum analyzer. The power is measured with three different resolution bandwidths

cal spectrum analyzer. Table 4.1 shows the signal powers measured at different resolution bandwidths. The high signal power supports the idea that the system

is limited by self phase modulation. The higher input power into span 1 is due to the higher loss. The effect of the Raman pump was however to reduce the effects of fibre non-linearities due to the lower input power as seen in table 4.2.

RB [*nm*]	Span 1	Span 2
0.5	1.9dBm	-0.4dBm
1	4.1dBm	1.6dBm
2	6.1dBm	3.7dBm

Tab. 4.2: The optimal signal input power into the spans with Raman amplifi-
cation measured using an optical spectrum analyzer. The power is
measured with three different resolution bandwidths

Due to the high level of dispersion compensating the effects of SPM is ex-
pected to be most severe at the beginning of the fibre span due to the high
peak power. The accumulated dispersion after 16 spans including the disper-
sion of the trimming fibre is $-7.2ps/nm$; again lower than $-14ps/nm$, which
is still higher than the expected lower bound of the dispersion tolerance of the
experiments. Thus there is some indications that the system still is limited by
non-linear effects. It is seen that there is no indications of an error floor occur-
ring on the BER curves shown in figure 4.11. However it seems that the BER
curve for four spans shown in green is erroneous.
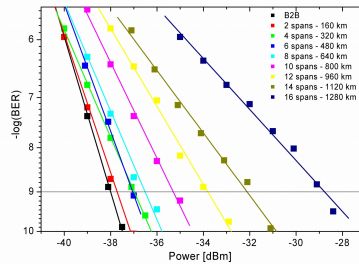
Fig. 4.11: The penalty vs. transmission length is shown.

Results 160*km* span experiment

In figure 4.12(a) the dispersion maps for the 160*km* spans is shown. All the
spans were pumped counter directionally. Figure 4.12(b) shows the BER curves

measured. As indicated on figure 4.12(a) the Raman on/off gain was largest for the post-compensation scheme due to the higher gain efficiency of the DCF, furthermore it is seen that most of the Raman gain in the symmetrical and pre-compensation schemes is in the $80km$ of transmission fibre. From the BER

(a) Spans   (b) BER
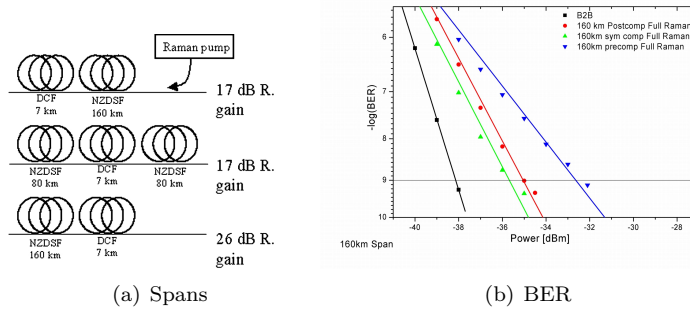
Fig. 4.12: (a) shows the BER curve for the experiment with additional disper-
          sion compensation. In (b) the BER is shown from which the power
          penalty can be deduced.

curves it is seen that the symmetrical scheme gave the best performance in accordance with similar investigations, whereas the pre-compensation scheme performed worst. It was not possible to transmit without Raman amplification for any of the three spans due to the very high span losses of $44dB$, i.e. the spans were noise limited without the Raman pump.

4.1.3   Discussion

The experiments performed at COM has shown that Raman pumping is beneficial due to an increased optical signal to noise ratio [46]. In the first series the transmission was mainly limited by the large residual dispersion of the fibre span used. A transmission of one single channel $40Gbit/s$ RZ over $800km$ of TW-RS using close to 100% slope compensation was achieved in the second experiment without the use of Raman amplification. The fibre non-linearities limited transmission due to the high input powers. Raman amplification allowed a lower input power due to improved signal to noise ratio, thus allowing a longer transmission distance of $1280km$.

4.2   160Gbit/s transmission

The transmission experiments at $160Gbit/s$ were all performed at the Heinrich Hertz Institute in Berlin. The work was done in collaboration with the "Optische Signalverarbeitung" group headed by Professor H.G. Weber. In particular a close collaboration with Dr. Jörn Berger, Mr. Sebastian Ferber, and Mr. Vincent Marembert was cherished. The latter two were also Ph.D. Students. The purpose of the work was to experimentally investigate the performance of different fibre types in a single channel $160Gbit/s$ transmission system. Four different fibre types given in table 4.3 were investigated. The same set-up was used in all experiments in order to compare the different performance due to fibre properties. In table 4.3 The dispersion and non-linear coefficient of the transmission fibre and dispersion compensating fibre are given.

Fibre	SLA	SMF	TW-REACH	TW-RS
$\frac{n_2}{A_{eff}}$ $[10^{-9}W^{-1}]$	0.22	0.30	~ 0.42	0.44
D $[ps/(nm \cdot km)]$	20	17	7.5	4.5
DCF	IDF$\times$2	EWB-DK	HS-DK	EHS
$\frac{n_2}{A_{eff}}$ $[10^{-9}W^{-1}]$	0.76	~ 1.6	1.8	1.8
D $[ps/(nm \cdot km)]$	-40	-120	-95	-120

Tab. 4.3: A resume of some important parameters for the fibres used in the experiments.

A theoretical study of the optimum fibre for high bit rate transmission suggests that a fibre with high dispersion would have a better performance than a low fibre dispersion [47]. The simulation used a commercially available simulation tool to solve the non-linear Schrödinger equation, where the time had been scaled with the pulse width, which was defined by a fixed duty cycle of 0.3. The calculated eyeopening penalties were plotted against DB^2 where D is the dispersion parameter and B is the bitrate i.e the dispersion length since $L_D \propto DB^2$. The parameters for the DCF and fibre non linearity were fixed. Further the effect of third order dispersion was neglected, which is not expected to cause any severe changes to the prediction of the study presupposing some slope compensation is used in a real system. However as seen in table 4.3 the fibre non-linear coefficient does vary with fibre dispersion, though only by a factor of two in the fibres shown.

4.2.1   Experimental Set-up

In this section the experimental set-up for the $3 \times 80km$ $160Gbit/s$ transmission experiments is described. A schematic of the transmitter is shown in figure 4.13. The 40Hz pulse train is made by optical time division multiplexing a $10GHz$ pulse train from a tuneable modelocked laser with a $1.4ps$ Sech^2 pulse shape. The wavelength of the signal was $1555nm$. The $40GHz$ pulse train is modulated using a LiNbO$_3$ modulater, which was driven by a $2^7 - 1$ pseudo random bit sequence (PRBS) generated by a bit pattern generator. The $40Gbit/s$ modulated signal is multiplexed to a single polarization $160Gbit/s$ channel. The PRBS sequence was retained in the $160Gbit/s$ signal by proper alignment of the delay of the 40 to 160 multiplexer. The signal was then launched into the fibre spans. The point labeled B2B in figure 4.13 was used as the transmitter back to back point. A polarisation controller was used to control the input state of polarization and thus mitigate the effect of polarization mode dispersion in the spans [33].
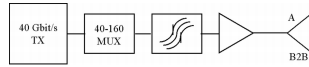
Fig. 4.13: The transmitter used in the $160Gbit/s$ transmission system experiments.

Figure 4.14 shows the span configuration used in the experiments. Signal was amplified before launched into the fibre spans. The average power level into the DCM was kept constant at $0dBm$ for all the modules in the spans, before the last DCM a short piece of SMF was inserted to trim the accumulated dispersion of the spans. The penalty as a function of input average power into the spans was measured. In the experiment involving the SLA and IDF×2 the set-up was a bit different; the amplifiers before the DCM were omitted due to the lack of DCM in this experiment.

At the receiver shown schematicaly in figure 4.15 the transmitted $160Gbit/s$ signal was demultiplexed to a $40Gbit/s$ tributary using an rf driven electro absorption modulator (EAM) in a self cascaded scheme [48] where the signal is passed through the EAM twice. Cascaded EAMs have previously been used to improve the peformance of the EAM. The demultiplexed signal is amplified and filtered using a $2.6nm$ filter, and amplified again. The amplified signal with average power of $8dBm$ is detected by an ultrafast photodiode[1] with a

---

[1] The diode was from u^2t photonics AG
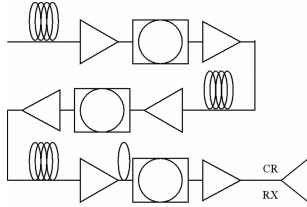
Fig. 4.14: The span configuration used in the $160Gbit/s$ transmission system experiments.

$40GHz$ bandwidth. The photodiode was connected directly to the bit error rate analyzer, which counted the errors. The clock for synchronizing the data and the bit error rate test set was transmitted at a separate wavelength as in the experiment performed at COM.
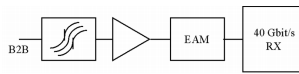
Fig. 4.15: The receiver used in the $160Gbit/s$ transmission system experiments.

Due to limited time only the BER vs. input power to the spans were measured in the following experiments.

4.2.2   SMF–EWBDK

The first experiment performed was on the standard single mode fibres. The fibre for the spans used was kindly prepared by the colleagues at OFS Fitel Denmark. The EWBDK[2] fibres were completed at OFS whereas the SMF spans were spliced at HHI. The residual dispersion of the spans was $-42ps/nm$ in total which requires approximately $2.4km$ of additional SMF to trim the dispersion. At a relatively low input power into the spans the dispersion was trimmed by measuring the pulse width of a $10GHz$ transmitted pulsetrain. The FWHM pulse width on the autocorrelator was minimized to $1.62ps$ by adding $\sim 2.9km$ SMF before the last DCM. The estimated residual dispersion with the added length of SMF was $2.5ps/nm$. The loss of the spans including splice loss was $16dB$ and the insertion loss of the DCM was $6dBm$.

---

[2] EWBDK stands for extra wide band dispersions kompenserende
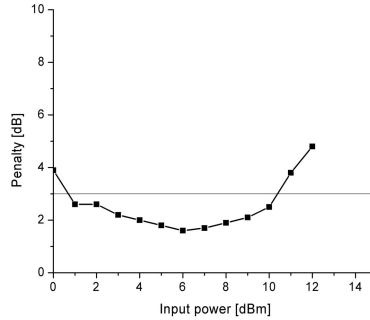
Fig. 4.16: The Penalty curve for the SMF/EWBDK spans after $240km$.

Figure 4.16 shows the obtained penalty curve for the SMF spans. It is seen that the penalty is below $3dB$ for a wide range ($11dB$) of input powers ($0.6dBm$–$10.4dBm$) and that a minimun penalty of $1.6dB$ at $6dBm$ input power into the spans was obtained showing a good perfomance.

The input power into the DCM was kept constant at $0dBm$ in order to avoid non-linear impairment arising from the DCF. The input power into the DCM was tested briefly to assure that there was no non-linear effects arising from the DCF. The input power into the spans was set to $6dBm$ while the DCM input power were increased in steps of $1dB$ until $4dBm$; no significant changes to the system performance were detected. Thus it was concluded that the possible non-linearities arising from the DCM were negligible with a $0dBm$ DCM input power.

4.2.3   TW-RS–EHS

The TW-RS spans were borrowed from COM and comprised of the two spans used in the previous experiments presented in section 4.1.1 and 4.1.2. A third span was included with a slightly worse dispersion compensation ratio than the first two, resulting in a residual dispersion of $-7.3ps/nm$ at $1555nm$. Additional $560m$ of SMF was added giving a $2.4ps/nm$ residual dispersion. The pulse width from the spans was $1.64ps$ with the added length of SMF. The insertion losses of the spans were $18dB$, and the insertion losses of the DCM were $4dB$. It is seen from figure 4.17 that the $3dB$ input power range is $5dB$ ($3dBm$–$8dBm$). The lowest penalty obtained was $2.5dB$ for the TW-RS/EHS spans. The low
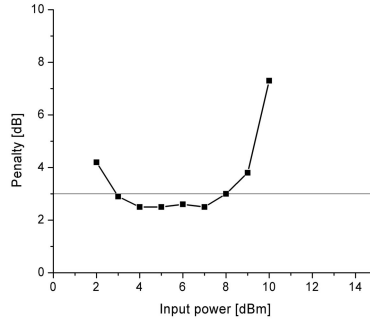
Fig. 4.17: The Penalty curve for the TW-RS/EHS spans after 240km.

$3dB$ range might be due to the high losses of the TW-RS spans. A wider range would thus be expected with better spans in terms of span loss.

4.2.4 TW-REACH–HSDK

The TW-REACH fibres were selected by the colleagues at OFS Fitel Denmark and spliced at HHI. The span losses of these spans were only 17.1dB compared to the 22dB for the TW-RS spans. 600m of additional SMF were added to minimize the pulse width from the span. The resulting pulse width was 1.57ps. The RDS of the HSDK fibre was selected to provide slope compensation. The residual dispersion of the spans was 1.2ps/nm. During the measurements on the TW-REACH the system was quite unstable due to the sensitivity on the ambient temperature changes of the de-multiplexer, in fact furher investigations showed a clear correlation between the on/off cycles of the air conditioning installation and the performance of the demultiplexer. However a measurement of the penalty was obtained which is shown in figure 4.18. The step in the low input part of the penalty curve could be ascribed erroneous measurement due to the instability of the system. It could be speculated that due to variations of the de-multiplexer the system sensitivity could have changed during a measurement. Since the insertion losses are lower for the TW-REACH spans it would be expected that the TW-REACH were less affected by noise at higher input powers. However the lowest penalty obtained was 2dB. The 3db penalty range is 5dB, however if the deterioration of the step is disregarded the 3dB range could be estimated as 8dB.
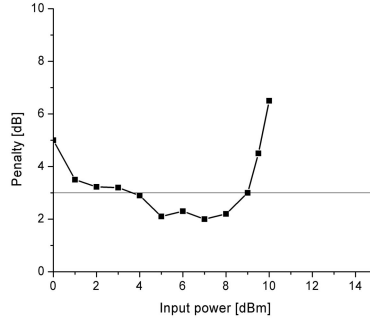
Fig. 4.18: The Penalty curve for the TW-REACH/HSDK spans after 240*km*.

4.2.5   SLA-IDF×2

The SLA-IDF×2 were carefully matched both in terms of slope but also in terms of length using the equations 2.29 and 2.30. The total resulting residual dispersion of the spans were $1.9ps/nm$. $180m$ of SMF was added in order to achieve a pulse width of $1.6ps$ after the spans. Thus a total residual dispersion including the added SMF was $5.0ps/nm$. During the measurements an opportunity to measure the total dispersion of the spans arrived due to an external visit from Perkin Elmer. The result was $4.7ps/nm$ corresponding well to the estimated value. Figure 4.19 shows the penalty curve for the SLA-IDF×2 experiment. A
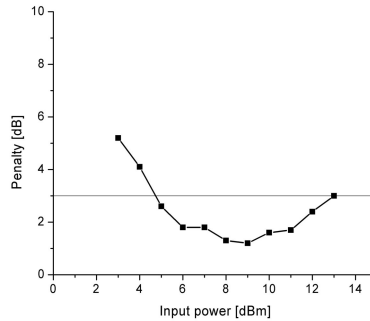
Fig. 4.19: The Penalty curve for the SLA-IDF×2 spans.

very high tolerance to non-linearity is seen as a $3dB$ penalty occurs at an input power as high as $13dBm$. Further the lowest penalty obtained was only $1.2dB$. However du to a high span loss of $20dB$ poor performance at lower powers was observed. Due to limited time at the time of preparing the spans the SLA fibres had a larger attenuation than expected. Thus a better performance at lower launch powers is expected. In fact it is seen from figure 4.20 that the difference of the $3dB$ penalty point for the lower input power is $4dB$ accordingly to the difference in the span losses of $4dB$. A numerical simulation showing excel-
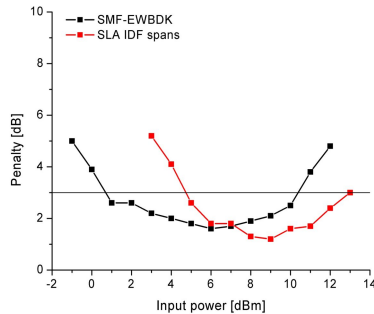
Fig. 4.20: The Penalty curve for the SMF EWBDK spans.

lent correspondence with the experimental result shown in figure 4.20 has been performed in [49]. Thus the same performance at lower input powers for the SLA-IDF$\times$2 as the SMF/EWBDK can be expected promising a very wide $3dB$ penalty range of $12dB$.

4.2.6   Discussion

A $3 \times 80km$ single channel with a line rate of $160Gbit/s$ experiment comparing four different types of fibres were performed. Successful transmission of $160Gbit/s$ signal over $240km$ was achieved on all fibre types. Figure 4.21(a) shows a resume of the results given in the previous sections. The results are ordered by the fibre dispersion with the lowest dispersion first. The TW-RS is shown in the black curve, the TW-REACH is shown in red, the green curve depicts the SMF, and finally the blue curve represents the SLA-IDF$\times$2 results. It is interesting to note that comparing the $3dB$ penalty point at lower input power of the SMF case, which shows the better performance, the differences cor-

respond very well with the difference in span loss, except for the TW-REACH results. However disregarding the step and interpolating it is seen that the virtual intersection does correspond very well with the difference in the span loss. This is also what was expected prior to the experiments since the exact same system was used in the experiments only the fibres were changed, i.e. noise performance should be comparable. Thus it is suggested that the low power performance of the non-zero dispersion shifted fibres could be improved by lowering fibre attenuation.
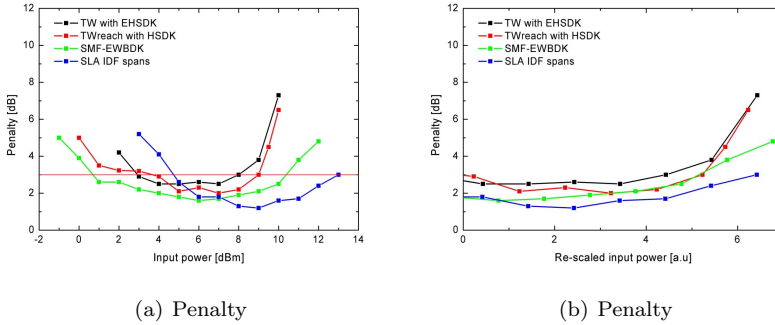
(a) Penalty   (b) Penalty

Fig. 4.21: (a) shows the penalty curves for the all the experiments. In (b) the same penalties are shown vs. $\frac{n_2 P_{in}}{A_{eff}}$ using a logarithmic scale.

The lowest penalty obtained depends on the dispersion. The higher the local dispersion the lower the penalty. It is clear that the high power performance is very different for the different fibre type. Since the non-linear coefficient is lower for the fibres with high dispersion as seen in table 4.3 the dynamics of the dispersion and fibre non-linearity is not perfectly clear. In figure 4.21(b) the system penalty is shown against $\frac{n_2 P_{in}}{A_{eff}}$. It is seen that when the input power is re-scaled with the non-linear coefficient the behaviour at high powers become almost identical. Especially the curves for the TR-RS and the TW-REACH shows identical behaviour. In fact all the curves tend to increase around 3–5 on the arbitrary power scale used. The SMF and SLA do not increase as rapidly as the non-zero dispersion shifted fibres due to the higher dispersion. The slower increase of the penalty for the SMF and SLA-IDF$\times$2 verifies that the minimum penalties obtained are representative for the measurements and not just an artifact from the measurements.

4.3   Summary

In this chapter single channel systems experiments at both $40Gbit/s$ and $160Gbit/s$ have been presented. Raman amplification was deployed and shown to be beneficial due to the improved noise performance. $1280km$ $40Gbit/s$ transmission over TW-RS fibre using EHS DCM was achieved in a re-circulating loop experiment implementing Raman amplification. Really good dispersion compensation suited for both $40Gbit/s$ and $160Gbit/s$ transmission rates were demonstrated.

Furthermore an investigation of the performance of four different fibre types in a $160Gbit/s$ transmission set-up was presented for the first time. The result showed that high numerical dispersion is preferable at $160Gbit/s$ bit rates reducing intrachannel non-linear effects effectively in agreement with theoretical studies. Furthermore the results showed that the performance at high input power scaled nicely with the inverse non-linear length; $\frac{n_2 P_{in}}{A_{eff}}$.

5. CONCLUSION

In this chapter a resume of the results obtained is given along with some concluding remarks.

5.1   Dispersion compensation

In first chapter chromatic dispersion was considered. Higher order dispersion has been discussed in order to determine its influence on $160Gbit/s$ systems. The peculiar pulse shapes due to the third order dispersion were explained physically. The effect of fourth order dispersion was also explained. It was established that even though the third order dispersion length was much longer than the dispersion length it still was comparable to the transmission lengths used in optical communications systems. Thus in dispersion compensated systems the accumulated effects of third order dispersion must be compensated, prompting the necessity of slope compensation fibres. However the tolerance of the third order dispersion was argued to be much less stringent than the tolerance for the chromatic dispersion which was estimated to be around $\pm 2ps/nm$ for systems with a pulse width of $1.56ps$, for longer pulses the tolerance could be relaxed somewhat. The tolerance for the slope was estimated to be $\pm 2ps/nm^2$. For WDM purposes the requirement of the slope compensation was argued to be tighter than the requirements for compensation of the third order dispersion, due to the broader bandwidth needed for WDM system. The bandwidth of a $160Gbit/s$ channel is roughly $5nm$ compared to $50nm$–$100nm$ for WDM based systems. The fourth order dispersion was negligible at $160Gbit/s$, however expected to be important at even higher transmission rates. Due to the low residual dispersion tolerance of 160Gbit/s 100% slope compensation over a very broad wavelength range is necessary for WDM experiments at a rate of 160Gbit/s

Dispersion compensation using fibres, was discussed briefly and a PMD figure of merit was introduced, in order provide an easy way of estimating the

differential group delay of a dispersion compensating module from the desired total dispersion. The PMD FOM is a good parameter for evaluating the PMD of a DCF. The design of a slope compensation module was briefly discussed and it was seen that the dispersion of the fibre should be designed so that the inflexion point of the dispersion curve should be in the middle of the dispersion range used. Furthermore the RDS curve of the DCF should intersect the RDS curve of the transmission fibre twice and preferably the the point of maximum RDS in between the points of intersection. The broadest slope compensated range is achieved when the length of dispersion compensating fibre is matched at the middle wavelength with respect to the intersection wavelengths. The result for a slope compensating module for TW-RS based on the developed fibre called EHS was shown.

Due to the importance of the RDS for transmission systems at $160Gbit/s$ and WDM systems the measurement of the dispersion was investigated. Traditionally a fourth order polynomial or a 5-term Sellmeier has been used to measure the slope. It was shown that there were some great variations on the slope although no variations were seen on the fitted group delay curves by the naked eye. Furthermore a better precision was investigated. It was shown that re-scaling the abscissa to the range -1–1 before fitting improved the precision significantly. Furthermore it was shown that the fourth order polynomial and 5-term Sellmeier were inadequate as fitting functions to the measured dispersion for an EHS fibre. A polynomial of sixth degree proved adequate, and showed great agreement when compared with a measured curve for a span.

5.2   Fibre Non-linearity

In the second chapter an assessment of the effect of Raman amplification on the non-linear response of an optical fibre using some simple theoretical considerations and experimental verification has been shown.

Although XPM between pump and signal was neglected in this case the experimental data point fits very well with theory. Nevertheless in future experiments counter measures against SBS must be employed, and the theory must at least be expanded to entail the effects of pump depletion, which would introduce a slight dependency of the signal input power. However in most practical cases chromatic dispersion of the fibre cannot be neglected and must be incorporated in the theory.

Assuming that the only interaction between the pump and the signal is stimulated Raman scattering, no pump depletion, cw pump, negligible effect of

chromatic dispersion, and a slowly varying envelope it was shown that the non-linear enhancement factor, R_e, due to Raman amplification was independent on the signal input power. Furthermore tuning of R_e can easily be done by varying the power of the pump and by proper choice of pumping scheme. The non-linear enhancement is due to power evolution of the signal when Raman amplification is applied to the fibre.

An experiment using a 2.1km long HNLF, with $\frac{n_2}{A_{eff}} = 1.49 10^{-9} W^{-1}$ was performed to test the theory. The pump and signal wavelengths used were 1455nm and 1550nm respectively corresponding to a frequency shift of 12.6THz. Using a 382mW pump an enhancement factor of 3.8 was obtained. The Raman gain efficiency was measured for the test fibre resulting in $\frac{g_R}{A_{eff}} = 4.4 (Wkm)^{-1}$. A small discrepancy between theory and experiment was observed. This could be ascribed to the effects of pump depletion and SBS.

Raman amplification shows a great potential to enhance the fibre non-linearity and to realize devices for optical communication systems based on non-linear effects in optical fibres with dynamic control of the fibre non-linear response. However when taking chromatic dispersion into account the power of the pulse is lowered by the pulse broadening lowering the detrimental effect of fibre non-linearity.

5.3 System experiments

Raman amplification was deployed in the 40Gbit/s experiment and shown to be beneficial due to the improved noise performance. 1280km transmission over TW-RS fibre using EHS DCM was achieved in a re-circulating loop experiment implementing Raman amplification. Excellent dispersion compensation suited for both $40Gbit/s$ and $160Gbit/s$ transmission rates where demonstrated.

A comparison of four different fibre types SLA, SMF, TW-REACH, and TW-RS in a $160Gbit/s$ transmission experiment was shown. Non-linear effects of the DCM were minimized by keeping the input power into the DCM constant at $0dBm$. The results indicated in agreement with theoretical studies that high local dispersion is preferred at $160Gbit/s$ due to the effective suppression of intra channel non-linear interactions, which dominates in high speed transmission systems. The relative high bandwidth of a single channel and large channel spacing of a few hundreds of GHz required for WDM systems lead to a domination of the intra channel effect over the inter channel effects. Thus a system configuration showing good performance at a single channel promises a good performance at a WDM configuration as well.

5.4   Further work

Although $160Gbit/s$ transmission systems have been the subject of intense re-search activity there is still some uncharted road to be covered before the technology will be feasible enough for deployment in commercial systems. The main focus of this work has been fibre based chromatic dispersion and fibre non-linearity; topics such as polarization mode dispersion, broad band PMD mitigation, and adaptive dispersion are very important topics for the future transmission systems at $160Gbit/s$ or above. Furthermore future systems must deploy WDM technology in order to be competitive.

The non-linear degradation arising from a Raman amplified dispersion compensating module is a very interesting topic, which follows directly from the work already presented in this thesis. A modification of the model presented in chapter 3, which incorporates chromatic dispersion, could be a topic of further investigation in order to understand and quantify the added non-linear response of a Raman pumped dispersion compensating module.

REFERENCES

[1] Lars Gruner-Nielsen, Stig Nissen Knudsen, Bent Edvold, Torben Veng, Dorte Magnussen, C. Christian Larsen, and Hans Damsgaard. Dispersion compensating fibers. *Optical Fiber Technology*, 6(2):164–180, 2000.

[2] U. Feiste, R. Ludwig, C. Schubert, J. Berger, C. Schmidt, H.G. Weber, B. Schmauss, A. Munk, B. Buchold, D. Briggmann, F. Kueppers, and F. Rumpf. 160 gbit/s field transmission over 116 km standard single mode fibre using 160 gbit/s otdm and 40 gbit/s etdm demultiplexer. *Optoelectronics, IEE Proceedings-*, 148(4):171–175, 2001.

[3] B. Mikkelsen, G. Raybon, B. Zhu, R.J. Essiambre, P.G. Bernasconi, K. Dreyer, L.W. Stulz, and S.N. Knudsen. High spectral efficiency [0.53 bit/s/hz] wdm transmission of 160 gb/s per wavelength over 400 km of fiber. *Optical Fiber Communication Conference and Exhibit, 2001. OFC 2001*, page ThF2.1, 2001.

[4] Takashi Yamamoto, Eiji Yoshida, Kohichi R. Tamura, and Masataka Nakazawa. 100 km transmission of a 640 gbit/s otdm signal using femtosecond pulses. *Electronics and Communications in Japan, Part I: Communications (English translation of Denshi Tsushin Gakkai Ronbunshi)*, 85(5):48–56, 2002.

[5] S. Kawanishi, H. Takara, K. Uchiyama, I. Shake, and K. Mori. $3tbit/s(160gbit/s \times /19$ ch) otdm/wdm transmission experiment. *Optical Fiber Communication Conference, 1999. OFC/IOOC '99. Technical Digest*, page PD1/1, 1999.

[6] Lars Gruner-Nielsen, Stig Nissen Knudsen, Torben Veng, Bent Edvold, and C. Christian Larsen. Design and manufacture of dispersion compensating fibre for simultaneous compensation of dispersion and dispersion slope. *Conference on Optical Fiber Communication, Technical Digest Series*, 1999.

[7] N.T. Quang Le, T. Veng, and L. Gruner-Nielsen. New dispersion compensating module for compensation of dispersion and dispersion slope of non-zero dispersion fibres in the c-band. *Optical Fiber Communication Conference and Exhibit, 2001. OFC 2001*, 2:TuH5, 2001.

[8] Siddharth Ramachandran. Higher-order-mode dispersion compensation for broadband dispersion and non-linearity management in transmission systems. *Conference on Optical Fiber Communication, Technical Digest Series*, 70:333–335, 2002.

[9] A.H. Gnauck, L.D. Garrett, Y. Danziger, U. Levy, and M. Tur. Dispersion and dispersion-slope compensation of nzdsf over the entire c band using higher-order-mode fibre. *Electronics Letters*, 36(23):1946 –1947, 2000.

[10] C.D. Poole, J.M. Wiesenfeld, D.J. DiGiovanni, and A.M. Vengsarkar. Optical fiber-based dispersion compensation using higher order modes near cutoff. *Lightwave Technology, Journal of*, 12(10):1746 –1758, 1994.

[11] R.M. Jopson, A.H. Gnauck, and R.M. Derosier. Compensation of fibre chromatic dispersion by spectral inversion. *Electronics Letters*, 29(7):576–578, 1993.

[12] S. Watanabe, T. Naito, and T. Chikama. Compensation of chromatic dispersion in a single-mode fiber by optical phase conjugation. *IEEE Photonics Technology Letters*, 5(1):92–95, 1993.

[13] M.H. Chou, I. Brener, G. Lenz, R. Scotti, E.E. Chaban, J. Shmulovich, D. Philen, S. Kosinski, K.R. Parameswaran, and M.M. Fejer. Efficient wideband and tunable midspan spectral inverter using cascaded nonlinearities in linbo/sub 3/ waveguides. *IEEE Photonics Technology Letters*, 12(1):82 –84, 2000.

[14] T. Ito, Y. Yano, T. Ono, and K. Emura. Pre-chirp assisted normal dispersion region transmission for highly marginal dense wdm transoceanic system. *Conference on Optical Fiber Communication, Technical Digest Series*, pages 367–368, 1998.

[15] Thierry Georges and Benoit Charbonnier. Pre-chirping and dispersion compensation for long-haul 20-gbit/s soliton transmission at 1.55 μm on non-dispersion-shifted fibers. *Conference on Optical Fiber Communication, Technical Digest Series*, pages 144–145, 1997.

[16] Kerry Hinton. Long haul system issues with bragg fiber grating-based dispersion compensation. *Optical Fiber Technology*, 5(2):145–164, 1999.

[17] Hiroki Ooi, K. Nakamura, Y. Akiyama, T. Takahara, T. Terahara, Y. Kawahata, H. Isono, and G. Ishikawa. 40-gb/s wdm transmission with virtually imaged phased array (vipa) variable dispersion compensators. *Lightwave Technology, Journal of*, 20(12):2196–2203, 2002.

[18] H. Ooi, K. Nakamura, Y. Akiyama, T. Takahara, J. Kumasako, I.C. Rasmussen, T. Terahara, Y. Kawahata, H. lsono, G. Ishikawa, and N. Yamaguchi. 3.6-tbit/s (43-gbit/s x 88 ch) transmission over 600 km nzdsf with vipa variable dispersion compensators. *Optical Fiber Communication Conference and Exhibit, 2002. OFC 2002*, pages 555–556, 2002.

[19] Jr. Cimini, L.J., L.J. Greenstein, and A.A.M. Saleh. Optical equalization for high-bit-rate fiber-optic communications. *IEEE Photonics Technology Letters*, 2(3):200–202, 1990.

[20] Jr. Cimini, L.J., L.J. Greenstein, and A.A.M. Saleh. Optical equalization to combat the effects of laser chirp and fiber dispersion. *Lightwave Technology, Journal of*, 8(5):649–659, 1990.

[21] M. Amemiya. Pulse broadening due to higher order dispersion and its transmission limit. *Lightwave Technology, Journal of*, 20(4):591–597, 2002.

[22] F. Futami, K. Taira, K. Kikuchi, and A. Suzuki. Wideband fibre dispersion equalisation up to fourth-order for long-distance subpicosecond optical pulse transmission. *Electronics Letters*, 35(25):2221–2223, 1999.

[23] M.D. Pelusi, Y. Matsui, and A. Suzuki. Fourth-order dispersion suppression of ultrashort optical pulses by second-order dispersion and cosine phase modulation. *Optics Letters*, 25(5):296–8, 2000.

[24] Govind P. Agrawal. *Nonlinear Fiber optics*. Optics and Photonics. Academic Press, 2.nd edition, 1989.

[25] R.H. Stolen, J.P. Gordon, W.J. Tomlinson, and H.A. Haus. Raman response function of silica-core fibers. *Journal of the Optical Society of America B (Optical Physics)*, 6(6):1159–66, 1989.

[26] K.J. Blow and D. Wood. Theoretical description of transient stimulated raman scattering in optical fibers. *Quantum Electronics, IEEE Journal of*, 25(12):2665–2673, 1989.

[27] Govin P. Agraval. *Fiber-Optic communication systems.* Microwave and Optical Enginering. John Wiley & Sons, 2.nd edition, 1997.

[28] Lars Grüner-Nielsen. *High Index Fibres.* PhD thesis, Technical University of Denmark, May 1998.

[29] R.J. Nuyts, Yong Kwan Park, and P. Gallion. Dispersion equalization of a 10 gb/s repeatered transmission system using dispersion compensating fibers. *Lightwave Technology, Journal of,* 15(1):31–42, 1997.

[30] M. Wandel, T. Veng, N.T. Quang Le, and L. Gruner-Nielsen. Dispersion compensating fibre with a high figure of merit. *Proceedings - Post-Deadline Papers. 27th European Conference on Optical Communication (Cat. No.01TH8551),* pages 52–3 vol.6, 2001.

[31] F. Forghieri, R.W. Tkach, and A.R. Chraplyvy. Dispersion compensating fiber: Is there merit in the figure of merit? *IEEE Photonics Technology Letters,* 9(7):970 –972, 1997.

[32] Stig Nissen Knudsen. *Optmization of Fibers Used for Dispersion Compensation in WDM systems.* PhD thesis, Technical University of Denmark, June 2002.

[33] Henrik Sunnerud. *Polarization-mode dispersion in optical fiber:characterization,transmission, and compensation.* PhD thesis, Chalmers University of Technology, March 2001.

[34] A. Galtarossa, L. Palmieri, and A. Pizzinat. Optimized spinning design for low pmd fibers: an analytical approach. *Lightwave Technology, Journal of,* 19(10):1502–1512, 2001.

[35] L. Leng, B. Zhu, S. Stolz, L.E. Nelson, Quang Le, and L. Gruner-Nielsen. 1.6 tb/s (40 x 40 gb/s) transmission over 500 km of nomero dispersion fiber with 100-km amplified spans compensated by extra-high-slope dispersion-compensating fiber. *Optical Fiber Communication Conference and Exhibit, 2002. OFC 2002,* pages 554–555, 2002.

[36] W.A. Gambling, H. Matsumura, and C.M. Ragdale. Mode dispersion, material dispersion and profile dispersion in graded-index single-mode fibres. *IEE Journal on Microwaves, Optics and Acoustics,* 3(6):239–46, 1979.

[37] A. Boskovic, S.V. Chernikov, J.R. Taylor, L. Gruner-Nielsen, and O.A. Levring. Direct continuous-wave measurement of n/sub 2/ in various types of telecommunication fiber at 1.55 mu m. *Optics Letters*, 21(24):1966–8, 1996.

[38] D. Derrickson. *Fiber Optic Test And Measurement*. Hewlett-Packard proffessional books, 1998.

[39] C V Raman and K S Krishnan. Section i : Reprints - a new class of spectra due to secondary radiation. part i. *Indian Journal of Physics and Proc of the Indian Assoc for the Cultivation of Science - A*, 73(1SPECI):21–42, 1999.

[40] C. Fludger, A. Maroney, N. Jolley, and R. Mears. An analysis of the improvements in osnr from distributed raman amplifiers using modern transmission fibres. *Optical Fiber Communication Conference, 2000*, 4:100–102 vol.4, 2000.

[41] T. Yamamoto, U. Feiste, J. Berger, C. Schubert, C. Schmidt, R. Ludwig, and H.G. Weber. 160 gbit/s demultiplexer with clock recovery using soa-based interferometric switches and its application to 120 km fiber transmission. *Optical Communication, 2001. ECOC '01. 27th European Conference on*, 2:192–193 vol.2, 2001.

[42] R.-J. Essiambre, B. Mikkelsen, and G. Raybon. Intra-channel cross-phase modulation and four-wave mixing in high-speed tdm systems. *Electronics Letters*, 35(18):1576–1578, 1999.

[43] N.S. Bergano and C.R. Davidson. Circulating loop transmission experiments for the study of long-haul transmission systems using erbium-doped fiber amplifiers. *Lightwave Technology, Journal of*, 13(5):879–888, 1995.

[44] Jianjun Yu, Yujun Qian, P. Jeppesen, and S.N. Knudsen. Broad-band and pulsewidth-maintained wavelength conversion based on a high-nonlinearity dsf nonlinear optical loop mirror. *IEEE Photonics Technology Letters*, 13(4):344 –346, 2001.

[45] Alvaro Buxens. *40Gb/s optical transmission systems*. PhD thesis, Technical University of Denmark, February 2003.

[46] Y. Qian, Q. Le, W. Wang, B. Pálsdóttir, and C.G. Jørgensen. Optimized dipersion compensating raman amplifier with respect to linear and nonlinear impairments. *Optical Fiber Communication Conference and Exhibit, 2003. OFC 2003*, 2003.

[47] B. Konrad and K. Petermann. Optimum fiber dispersion in high-speed tdm systems. *IEEE Photonics Technology Letters*, 13(4):299–301, 2001.

[48] E. Hilliger et. al. *Optical Fiber Communication Conference and Exhibit, 2003. OFC 2003*, page TUP2, 2003.

[49] J. Berger, Q. Le, A. Wietfeld, S. Ferber, L. Grüner-Nielsen, B. Schmauss, and H.G. Weber. 160gbit/s transmission over dispersion managed fibre set. *Submitted to ECOC*, page 2, 2003.

[50] B.I Bleaney & B.Bleaney. *Electricity and Magnetism*, volume 1. Oxford University Press, 3.rd edition, 1976.

APPENDIX

A. NON-LINEAR SCHRÖDINGER EQUATION

In this appendix the non-linear Schrödinger equation is derived. Taking the starting point from Maxwells equations, which can be found in almost any textbook on classical electromagnetism e.g. [50], it can be shown that optical waves are governed by the wave equation A.1.

$$(A.1) \quad \nabla^2 E - \left(\frac{n}{c}\right)^2 \frac{\partial^2 E}{\partial t^2} = 0$$

where n is the refractive index of the medium in which the optical wave is propagating, c is the vacuum speed of light, t is the time, and E is the complex representation of the wavefunction. Since $\nabla^2 = \frac{\partial^2}{\partial x^2} + \frac{\partial^2}{\partial y^2} + \frac{\partial^2}{\partial z^2}$ is a linear operator the wave equation A.1 is a linear partial differential equation assuming that n is independent of E. In optical fibres the system of reference is almost always chosen so that the optical field propagates in the direction of the cartesian coordinate z and the remaining coordinates can be disregarded. Thus the equation A.1 can be simplified into equation A.2 due to the choice of frame of reference.

$$(A.2) \quad \frac{\partial^2}{\partial z^2} E - \left(\frac{n}{c}\right)^2 \frac{\partial^2 E}{\partial t^2} = 0$$

A.1 Linear dispersion

Due to the linearity of equation A.2 the superposition of any solutions to equation A.2 will always be a solution to equation A.2. Therefore the following discussion will take a starting point in a monochromatic wave which can be described as.

$$(A.3) \quad E(z,t) = E(z) \exp(-i\omega t)$$

where ω is the angular frequency of the optical wave. Inserting equation A.3 into equation A.2 an equation governing the complex amplitude, $E(z)$, can be

found.

(A.4) $\left(\dfrac{\partial^2}{\partial z^2} + \beta^2\right) E(z) = 0$

The dependence of the wavenumber, β, to ω is determined by the dispersion relation:

(A.5) $\beta(\omega) = \dfrac{n(\omega)\omega}{c}$

where frequency dependence of the refractive index has been written out explicitly. In optical fibres the refractive index is not determined by the optical properties of the material alone but also by wave-guide and index profile effects due to the actual design of the fibre, thus the refractive index used is actually the effective refractive index of the fibre.

The information stream of an optical transmission system is always carried by an optical field with a finite frequency bandwidth at one or more given carrier frequencies. It is convenient to express the optical field in terms of the carrier frequency. In order to illustrate this a superposition of two plane waves separated by a small frequency difference is contemplated. For simplicity the amplitude of the two plane waves are considered to be equal in magnitude.

(A.6) $E(z,t) = A\left[\exp(i(\beta(\omega_0)z - \omega_0 t) + \exp(i(\beta(\omega_1)z - \omega_1 t))\right]$

Expressing the optical field in equation A.6 in terms of ω_0 is done by setting $\omega_1 = \omega_0 + \Delta\omega$ and inserting the expression for ω_1 into equation A.6. Since $\Delta\omega \ll \omega_0$ in most practical cases $\beta(\omega_1) = \beta(\omega_0 + \Delta\omega)$ can be expressed by a Taylor series, where terms up to the order of two are retained

(A.7) $E(z,t) = A\left[1 + \exp(i(\beta_1\Delta\omega + \tfrac{1}{2}\beta_2\Delta\omega^2)z - \Delta\omega t)\right]\exp(i(\beta_0 z - \omega_0 t))$

where $\beta_n = \dfrac{d^n\beta}{d\omega^n}\big|_{\omega=\omega_0}$. Since $\Delta\omega \ll \omega_0$ the term in the square brackets varies much slower than the rightmost term outside the square brackets. The rapid varying term can be omitted because variations at optical frequencies cannot be detected with the current status of the high speed electronic technologies. Thus it is sufficient to express the information stream by modeling the slowly varying envelope of the optical field, which can be detected at least for transmission rates below 40Gbit/s. Introducing the retarded time $T = t - \beta_1 z$ and omitting the rapid varying part of equation A.7 the slowly varying envelope can be expressed

in a simple and instructive way. Using the retarded time is not equivalent with using a frame of reference moving with the velocity β_1^{-1}. It is important to stress that the frame of reference is still the laboratory frame of reference, only the elapsed time when the field have propagated a distance z down the fibre is being subtracted for the sake of simplicity.

$$(A.8) \quad A(z, T) = A \left[1 + \exp(i(\frac{1}{2}\beta_2\omega^2 z - \omega T)) \right]$$

Where $A(z, T)$ denotes the slowly varying amplitude of the optical field. In equation A.8 ω is used to express the frequency difference of the optical field relative to the carrier frequency instead of $\Delta\omega$. Using this notation negative frequencies corresponds to frequencies lower than the carrier frequency. Remembering that the amplitudes of the fields where assumed to be of similar magnitude equation A.8 can be generalized to the case with N plane waves of different amplitudes.

$$(A.9) \quad A(z, T) = \sum_n^N a_n \exp(i(\frac{1}{2}\beta_2\omega_n^2 z - \omega_n T))$$

where a_n is the amplitude of the nth frequency, ω_n. In general $A(z, t)$ can be represented by an expansion of plane waves where the amplitudes of the individidual plane waves are the expansion coefficients. Equation A.9 shows that in the slowly varying envelope representation of the optical field, the phase velocity, β_0^{-1}, and group velocity, β_1^{-1}, are of no importance, whereas the second order term, β_2, and possible higher order terms plays a distinctive role. A further generalization to the discrete equation A.9 can be made.

$$(A.10) \quad A(z, T) = \int_{-\infty}^{\infty} d\omega a(\omega) \exp(i(\frac{1}{2}\beta_2\omega^2 z - \omega T))$$

where $a(\omega)$ is the amplitude distribution of the frequencies i.e. the spectrum of the optical field. The negative frequencies represents the frequencies below the carrier frequency. Apart from a normalization constant, equation A.10 is the inverse Fourier-transform of the optical spectrum, $a(\omega)$. The slowly varying envelope of the optical field satisfies another partial differential equation than equation A.4. By applying the operator $i\frac{\partial}{\partial z}$ on equation A.10 it is seen that the slowly varying envelope satisfies equation A.11.

$$(A.11) \quad i\frac{\partial A(z, T)}{\partial z} = \frac{\beta_2}{2}\frac{\partial^2 A(z, T)}{\partial T^2}$$

remembering that $FT^{-1}\{(i\omega)^n\} = \frac{\partial^n}{\partial T^n}$.

A.2   Non-linear term

So far only the linear part of the non-linear Schrödinger equation has been discussed. In this section the non-linear term is introduced. In an optical fibre the non-linear term arises from the third order susceptibility $\chi^{(3)}$. From an engineering point of view the effect of $\chi^{(3)}$, which is a third order tensor can be summarized in the nonlinear index n_2. The refractive index is thus given by equation A.12.

(A.12) $n = n_l + n_2 \dfrac{|A|^2}{A_{eff}}$

where A_{eff} is the effective area of the optical field. It is assumed that n_2 is independent of frequency. The dispersion relation in equation A.5 is thus modified by the addition of the n_2 as seen in equation A.13.

(A.13) $\beta(\omega) = \dfrac{n(\omega)\omega}{c} + \dfrac{n_2\omega|A|^2}{cA_{eff}}$

We now insert $\omega_1 = \omega_0 + \Delta\omega$ in equation A.13. Since the nonlinear effect is a small perturbation to the propagation constant $\beta(\omega)$ the term $\frac{n_2\Delta\omega|A|^2}{cA_{eff}}$ can be neglected. Thus equation A.7 becomes equation A.14 in the case where n_2 is considered.

(A.14)
$$A(z,t) = A\left[1 + \exp(i(\beta_1\Delta\omega + \tfrac{1}{2}\beta_2\Delta\omega^2 + \gamma|A|^2)z - \Delta\omega t)\right]\exp(i(\beta_0 z - \omega_0 t))$$

where $\gamma = \frac{n_2\omega_0|A|^2}{cA_{eff}}$. Following the procedure in section A.1 equation A.10 is modified to yield.

(A.15) $A(z,T) = \displaystyle\int_{-\infty}^{\infty} d\omega\, a(\omega)\exp(i(\tfrac{1}{2}\beta_2\omega^2 z + \gamma|A(z,T)|^2 z - \omega T))$

Applying the operator $i\frac{\partial}{\partial z}$ to equation A.15 the non-linear Schrödinger equation is obtained.

(A.16) $i\dfrac{\partial A(z,T)}{\partial z} = \dfrac{\beta_2}{2}\dfrac{\partial^2 A(z,T)}{\partial T^2} - \gamma|A(z,T)|^2 A$

where a term proportional to $\frac{\partial|A|^2}{\partial z}$ has been omitted because $\frac{\partial|A|^2}{\partial z} \ll |A|^2$ in the slowly varying envelope approximation. Equation A.16 is the governing

equation for the propagation of optical pulses in an optical fibre and is known as the non-linear Schrödinger equation.

The derivation of the non-linear Schrödinger equation given in this appendix is not completely correct. Although presented without any mathematical rigor the derivation given in section A.1 is physically and mathematically sound however, the non-linear part is not entirely waterproof since equation A.16 is non-linear the superposition principle does not hold i.e the sum of two solutions are not necessarily a solution as it is for the linear case. Since the non-linear coefficient is a small entity a perturbational approach should have been taken in the derivation given in section A.2.

B. CHIRP

In this appendix the effect of initial chirp is discussed in terms of a linearly chirped Gaussian pulse. It will be shown that the chirp is equivalent with dispersion.

B.1 Chirp

The effect of linear chirp is completely equivalent to the effect of chromatic dispersion. A linearly chirped Gaussian pulse can be described by the following equation [24]:

$$\text{(B.1)} \quad U(0,T) = \exp\left(-\frac{(1+iC)}{2}\left(\frac{T}{T_c}\right)^2\right)$$

Where T_c is the pulse width of the chirped pulse, and C is the chirp parameter. C is in fact equivalent with $x = \frac{z\beta_2}{T_c^2}$ as will be shown. The pulse broadening is determined by equation B.2

$$\text{(B.2)} \quad \frac{T}{T_c} = \sqrt{(1+Cx)^2 + x^2}$$

where $x = \frac{z}{L_D}$. It is seen that for $C\beta_2 > 0$ the pulse is broadened monotonous with x whereas the pulse is initially compressed to a minimum value before broadening again for the case $C\beta_2 < 0$. The minimal value of the pulse width is given by equation B.3 at a length given in equation B.4.

$$\text{(B.3)} \quad T_0 = T_{c,min} = \frac{T_c}{\sqrt{1+C^2}}$$

Here T_0 is the transform limited pulse width.

$$\text{(B.4)} \quad x_{min} = \frac{C}{1+C^2}$$

In order to establish a relation between the chirp parameter and β_2 it is instructive to look at the spectrum of the pulse.

The Fourier transform of the chirped Gaussian is given in equation B.5.

(B.5) $\tilde{U}(0,\omega) = \sqrt{\dfrac{2\pi T_c^2}{1+iC}}\, \exp\left(-\dfrac{\omega^2 T_c^2}{2(1+iC)}\right)$

where $\tilde{U}$ is the Fourier transform of U. Neglecting the amplitude for simplicity equation B.5 can be rewritten:

(B.6) $\tilde{U}(0,\omega) = \exp\left(-\dfrac{\omega^2 T_c^2(1-iC)}{2(1+C^2)}\right)$

The effect of β_2 in the frequency space can be taken from equation A.10.

(B.7) $\tilde{U}(0,\omega) = \exp\left(-\dfrac{\omega^2 T_0^2(1+i\beta_2\omega^2 z)}{2}\right)$

It is seen that equation B.6 and B.7 are identical if

(B.8) $C = -x = -\dfrac{z\beta_2}{T_0^2}$

and

(B.9) $T_c = T_0\sqrt{1+C^2} = T_0\sqrt{1+x^2}$

It is seen that the chirp from an anomalous fibre corresponds to a positive chirp parameter.

Equation B.9 corresponds to the pulse broadening of a transform limited Gaussian pulse due to β_2 as seen from equation B.2 were the chirp parameter is zero. In order to test the consistency of equations B.8 and B.9 the case of dispersion compensation is regarded. Taken for an example an optical pulse with transform limited pulse width, T_{TF}, and $\beta_2^{(TF)}$. After propagation of the length L_{TF} the dispersion induced chirp is: $C = -\dfrac{L_{TF}\beta_2^{(TF)}}{T_{TF}^2}$ and the pulse width, T_{DCF}, is given by equation B.9. The length of dispersion compensating fibre which gives the minimal pulse width is thus found from equation B.4.

(B.10) $\dfrac{L_{DCF}\beta_2^{(DCF)}}{T_{DCF}^2} = -\dfrac{L_{TF}\beta_2^{(TF)}}{T_{TF}^2}\dfrac{1}{1+C^2}$

inserting equation B.9 into equation B.10 and rearranging the result is.

$$(B.11) \quad L_{DCF}\beta_2^{(DCF)} = -L_{TF}\beta_2^{(TF)}\frac{1}{1+C^2}\frac{T_{TF}^2}{T_{DCF}^2} = -L_{TF}\beta_2^{(TF)}\frac{T_{TF}^2 T_{DCF}^2}{T_{TF}^2 T_{DCF}^2}$$

Giving the condition for dispersion compensation $L_{DCF}\beta_2^{(DCF)} + L_{TF}\beta_2^{(TF)} = 0$. Thus it is seen that initial linear chirp is equivalent to chromatic dispersion.

Furthermore equation B.2 provides an easy measurement of the chirp parameter of a Gaussian pulse, simply by measuring the pulse broadening at different lengths of fibres. Since for $x \gg 1$ equation B.2 is approximately $T_c = T_o\sqrt{1+C^2x^2}$

C. MATLAB CODE

In this appendix the MatLab code used for calculating the linear pulse propagation is presented. The linear part of the non-linear Schrödinger equation, in which the higher order terms up to fourth order is retained are taken as starting point.

$$\text{(C.1)} \quad i\frac{\partial A}{\partial z} = \left(\frac{1}{2}\beta_2\frac{\partial^2}{\partial T^2} + \frac{i}{6}\beta_3\frac{\partial^3}{\partial T^3} - \frac{1}{24}\beta_4\frac{\partial^4}{\partial T^4}\right)A$$

For simplicity the length can be represented in terms of the dispersion length, $L_D = \frac{T_0^2}{\beta_2}$ i.e $x = \frac{z}{L_D}$ and the retarded time normalized with T_0.

$$\text{(C.2)} \quad i\frac{\partial A}{\partial x} = \left(\frac{1}{2}\frac{\partial^2}{\partial \tau^2} + \frac{i}{6}\frac{\beta_3}{\beta_2 T_0}\frac{\partial^3}{\partial \tau^3} - \frac{1}{24}\frac{\beta_4}{\beta_2 T_0^2}\frac{\partial^4}{\partial \tau^4}\right)A$$

Equivalently with the dispersion length of β_2 dispersion lengths for β_3 and β_4 can be defined. As seen in equations C.3 and C.4.

$$\text{(C.3)} \qquad\qquad\qquad L_D^{(3)} = \frac{T_0^3}{\beta_3}$$

$$\text{(C.4)} \qquad\qquad\qquad L_D^{(4)} = \frac{T_0^4}{\beta_4}$$

$$\text{(C.5)}$$

Normalizing the dispersion lengths given in equations C.3 and C.4 with L_D it is seen that equation C.2 can be written as:

$$\text{(C.6)} \quad i\frac{\partial A}{\partial x} = \left(\frac{1}{2}\frac{\partial^2}{\partial \tau^2} + \frac{i}{6}\theta^{(3)}\frac{\partial^3}{\partial \tau^3} - \frac{1}{24}\theta^{(4)}\frac{\partial^4}{\partial \tau^4}\right)A$$

where $\theta^{(n)} = \frac{L_D}{L_{D^{(n)}}}$. This equation is the basis of the calculations shown in chapter 2. The main part of the MatLab code is given below:

```
clear all dtau=0.001;
%is the temporal resolution
taumax=100; tau=[-taumax/2:dtau:taumax/2];
%tau is the retarded time
B0=160;
%bitrate [Gbit/s]
b0=B0/1000;
%bitrate [Tbit/s]
r=0.25;
%The dutycycle
T0=r/b0;
%Is the pulse width described by r/B0 r is the duty cycle
%and B0 is the bitrate. [ps]

N=length(tau); omega=fftshift(2*pi/taumax*[-(N-1)/2:1:(N-1)/2]);
%the angular frequency

%pulse definition
amp=sqrt(1); %amplitude
offset=0;    %pulse temporal offset
chirp=0;     %pulse initial chirp

gpulse=gausspulse(tau,T0,amp,chirp); %Gaussian pulse definition
spulse=sechpulse(tau,T0,amp,chirp);  %sech squared pulse definition

x=2; %length normalized to dispersion length.
X=[0 0 1/2*T0^2*x 0 0];
%numerical solution
[cgpulse2,Pgpulse2]=dispprop(gpulse,X,omega);
[cspulse2,Pspulse2]=dispprop(spulse,X,omega);
dgpulse2=Pgpulse2/max(Pgpulse2);
dspulse2=Pspulse2/max(Pspulse2);
y=4; %length normalized to dispersion length.
Y=[0 1/6*T0^3*y  0 0 0];
%numerical solution
[cgpulse3,Pgpulse3]=dispprop(gpulse,Y,omega);
[cspulse3,Pspulse3]=dispprop(spulse,Y,omega);
dgpulse3=Pgpulse3/max(Pgpulse3);
dspulse3=Pspulse3/max(Pspulse3);
```

```
z=6; %length normalized to dispersion length.
Z=[1/24*T0^4*z 0 0 0 0];
%numerical solution
[cgpulse4,Pgpulse4]=dispprop(gpulse,Z,omega);
[cspulse4,Pspulse4]=dispprop(spulse,Z,omega) ;
dgpulse4=Pgpulse4/max(Pgpulse4);
dspulse4=Pspulse4/max(Pspulse4);

%analytical solution gauss
%[cdgauss,dgauss]=gauss_an_sol(t,x,T0,offset,amp,chirp)
```

The pulses are determined by the following functions:

Gaussian pulse definition

```
function pulse=gausspulse(tau,T0,u,chirp)

pulse=u.*exp(-(1+i*chirp)/2*(tau./T0).^2);
```

Hyperbolical secant pulse definition

```
function pulse=sechpulse(tau,T0,u,chirp)

pulse=u.*sech(tau./T0).*exp(-i*chirp/2*(tau./T0).^2);
```

The solution of the linear part of equation C.6.

```
function [outpulsec,outpulsepow]=dispprop(pulse,waveconst,omega)

outpulsec=ifft((fft(pulse).*exp(i.*polyval(waveconst,omega))));
outpulsepow=outpulsec.*conj(outpulsec);
```

The solution of the non-linear part of equation C.6.

```
function [outpulsec,outpulsepow]=nlprop(pulse,nlcoeff)

outpulsec=pulse.*exp(i*nlcoeff.*(pulse.*conj(pulse)));
outpulsepow=outpulsec.*conj(outpulsec);
```

The analytical solution for the dispersion of the Gaussian pulse in the case where only β_2 is included.

```
function [cdgauss,dgauss]=gauss_an_sol(t,x,T0,offset,amp,chirp)

cA=amp/sqrt(1-i*x*(1+i*chirp));
cdgauss=cA.*exp(-(t/T0).^2./(2*(1-i*x*(1+i*chirp)))*(1+i*chirp));
dgauss=cdgauss.*conj(cdgauss);
```